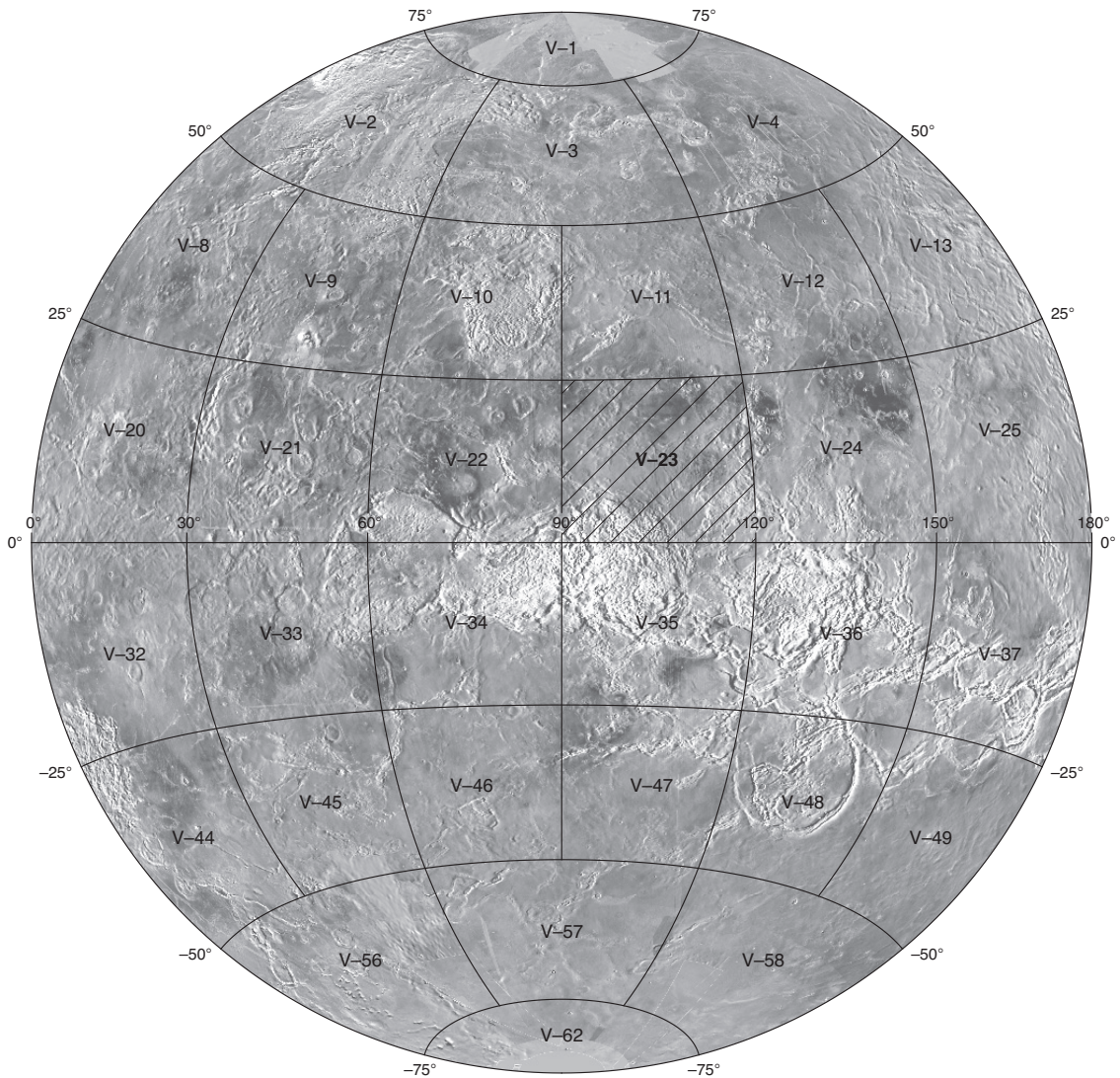


Prepared for the National Aeronautics and Space Administration

Geologic Map of the Niobe Planitia Quadrangle (V-23), Venus

By Vicki L. Hansen

Pamphlet to accompany
Scientific Investigations Map 3025



2009

U.S. Department of the Interior
U.S. Geological Survey

Contents

The Magellan Mission.....	1
Magellan radar data.....	1
Niobe Planitia quadrangle.....	1
Introduction.....	1
Image data	2
Image interpretation.....	2
Terminology.....	3
Geologic setting	3
Geologic relations.....	4
Basal terrain units.....	4
Tessera and intratessera terrain.....	4
Fracture terrain	6
Shield terrain material	6
23N/103E.....	6
21N/113E.....	7
13N/111E.....	7
23N/117E.....	7
13N/119E.....	7
Flow units	8
Flows originating within V-23.....	8
Rosmerta flows	8
Impact features.....	8
Tectonic structures.....	9
Regional structural suites	9
Regional extensional fractures	9
Wrinkle ridges	9
Inversion structures	9
Fabric anisotropy and implications for stress-strain relations	9
Coronae	10
Maya Corona	10
Dhisana Corona.....	10
Allatu Corona.....	11
Bhumiya Corona.....	11
Omeciuatl Corona	11
Rosmerta Corona	11
Formation of circular lows	12
Dorsa	12
Geologic history	13
Implications for Venus lowland resurfacing processes.....	14
Summary.....	16
References cited.....	18

Figure

2. Illustrations showing proposed evolution of Venusian surface.....	17
--	----

Tables

1. Numbers and densities of definite and combined shields.....	21
2. V-23 impact craters.....	22

The Magellan Mission

The Magellan spacecraft orbited Venus from August 10, 1990, until it plunged into the Venusian atmosphere on October 12, 1994. Magellan Mission objectives included (1) improving the knowledge of the geological processes, surface properties, and geologic history of Venus by analysis of surface radar characteristics, topography, and morphology and (2) improving the knowledge of the geophysics of Venus by analysis of Venusian gravity.

The Magellan spacecraft carried a 12.6-cm radar system to map the surface of Venus. The transmitter and receiver systems were used to collect three data sets: (1) synthetic aperture radar (SAR) images of the surface, (2) passive microwave thermal emission observations, and (3) measurements of the backscattered power at small angles of incidence, which were processed to yield altimetric data. Radar imaging and altimetric and radiometric mapping of the Venusian surface were accomplished in mission cycles 1, 2, and 3 from September 1990 until September 1992. Ninety-eight percent of the surface was mapped with radar resolution on the order of 120 m. The SAR observations were projected to a 75-m nominal horizontal resolution, and these full-resolution data compose the image base used in geologic mapping. The primary polarization mode was horizontal-transmit, horizontal-receive (HH), but additional data for selected areas were collected for the vertical polarization sense. Incidence angles varied between about 20° and 45°.

High-resolution Doppler tracking of the spacecraft took place from September 1992 through October 1994 (mission cycles 4, 5, 6). Approximately 950 orbits of high-resolution gravity observations were obtained between September 1992 and May 1993 while Magellan was in an elliptical orbit with a periapsis near 175 km and an apoapsis near 8,000 km. An additional 1,500 orbits were obtained following orbit-circularization in mid-1993. These data exist as a 75° by 75° harmonic field.

Magellan Radar Data

Radar backscatter power is determined by (1) the morphology of the surface at a broad range of scales and (2) the intrinsic reflectivity, or dielectric constant, of the material. Topography at scales of several meters and larger can produce quasi-specular echoes, and the strength of the return is greatest when the local surface is perpendicular to the incident beam. This type of scattering is most important at very small angles of incidence, because natural surfaces generally have few large tilted facets at high angles. The exception is in areas of steep slopes, such as ridges or rift zones, where favorably tilted terrain can produce very bright signatures in the radar image. For most other areas, diffuse echoes from roughness at scales comparable to the radar wavelength are responsible for variations in the SAR return. In either case, the echo strength is also modulated by the reflectivity of the surface material. The density of the upper few wavelengths of the surface can have a significant effect. Low-density layers, such as crater ejecta or volcanic ash, can absorb the incident energy and produce a lower observed echo. On Venus, a rapid increase in reflectivity exists at a certain critical elevation

above which high-dielectric minerals or coatings are thought to be present. This leads to very bright SAR echoes from virtually all areas above that critical elevation.

The measurements of passive thermal emission from Venus, though of much lower spatial resolution than the SAR data, are more sensitive to changes in the dielectric constant of the surface than to roughness. They can be used to augment studies of the surface and to discriminate between roughness and reflectivity effects. Observations of the near-nadir backscatter power, collected using a separate smaller antenna on the spacecraft, were modeled using the Hagfors expression for echoes from gently undulating surfaces to yield estimates of planetary radius, Fresnel reflectivity, and root-mean-square (rms) slope. The topographic data produced by this technique have horizontal footprint sizes of about 10 km near periapsis and a vertical resolution on the order of 100 m. The Fresnel reflectivity data provide a comparison to the emissivity maps, and the rms slope parameter is an indicator of the surface tilts, which contribute to the quasi-specular scattering component.

Niobe Planitia Quadrangle

Introduction

Niobe Planitia, namesake of the Niobe Planitia quadrangle (V-23), is named for Niobe, Queen of Thebes, married to King Amphion. Niobe was perhaps the most tragic figure of Greek mythology. In a bout of arrogance, Niobe bragged about her 14 children, mocking Leto who had only two children, Apollo (god of prophecy and music) and Artemis (virgin goddess of the wild). Upset by Niobe's mocking, Leto sent Apollo and Artemis to Earth to destroy Niobe's children; Apollo killed Niobe's seven sons and Artemis killed Niobe's seven daughters. In the heat of battle, King Amphion either committed suicide or was killed by Apollo. As a result of Niobe's haughtiness, her entire family died. Niobe fled to Mount Sipylus in Asia Minor where she turned to stone and her ceaseless tears formed a stream (the Achelous). Niobe, the symbol of eternal mourning, weeps to this day on Mount Sipylus, where a fading female image carved into a porous limestone cliff weeps after it rains.

The Niobe Planitia quadrangle (V-23) encompasses approximately 8,000,000 km² of the Venusian equatorial region extending from lat 0° to 25° N. and from long 90° to 120° E. (approximately 9,500 15-minute quadrangles on Earth). The map area lies along the north margin of the equatorial highland, Aphrodite Terra (V-35), and extends into the lowland region to the north, preserving a transition from southern highlands to northern lowlands (figs. 1, 2, map sheet). The northern parts of the crustal plateau, Ovda Regio and Haastse-baad Tessera, mark the south margin of the map area; Niobe and Sogolon Planitiae make up the lowland region. The division between Niobe and Sogolon Planitiae is generally topographic, and Sogolon Planitia forms a relatively small elongate basin. Mesolands, the intermediate topographic level of Venus, are essentially absent or represented only by Gegute Tessera, which forms a slightly elevated region that separates Niobe Planitia

from Llorona Planitia to the east (V-24). Lowlands within the map area host five features currently classified as coronae: Maya Corona (lat 23° N., long 97° E.) resides to the northwest and Dhisana, Allatu, Omeciuatl, and Bhumiya Coronae cluster loosely in the east-central area. Lowlands extend north, east, and west of the map area.

Mapping the Niobe Planitia quadrangle (V-23) provides an excellent opportunity to examine a large tract of lowlands and the adjacent highlands with the express goal of clarifying the processes responsible for resurfacing this part of Venus and the resulting implications for Venus evolution. Although Venus lowlands are widely considered to have a volcanic origin (Banerdt and others, 1997), lowlands in the map area lack adjacent coronae or other obvious volcanic sources.

Image Data

The Magellan Mission provided east-directed-illumination (left-looking, cycle 1), S-band (12.6 cm wavelength), and SAR images that cover over 80 percent of Niobe Planitia quadrangle (V-23) and nearly complete (~95%) coverage of right-looking (cycle 2) SAR; cycle 3 left-look stereo SAR coverage is not complete and is somewhat degraded in many locations across the map area (Ford and others, 1993). Digital Compressed Once Mosaicked Image Data Records (C1-MIDR; 275 m/pixel) SAR data from the regional data base and map base and the hardcopy full-resolution radar map (FMAP; 75 m/pixel) dataset were used in constructing the map, as well as digital, full-resolution (~75-125 m/pixel) SAR images downloaded from the Map-a-Planet web site (<http://pdsmaps.wr.usgs.gov/>). Ancillary data included the Global Topographic Data Record 3 (GTDR 3) that has an effective horizontal resolution of 10 km and similar products representing Fresnel reflectivity at 12.6-cm wavelength, average 1- to 10-m-scale slope, and derived 12.6-cm emissivity data (GRDR, GSDR, and GEDR, respectively). GTDR data were combined with SAR images to produce synthetic stereo anaglyphs (Kirk and others, 1992) using NIH-Image macros developed by D.A. Young. These images played a critical role in elucidating the relations between geology and topography and, in particular, the interaction of flows, primary and secondary structures, and topography.

Image Interpretation

The interpretation of features in Magellan SAR images is key to developing a geologic history for the Niobe Planitia quadrangle (V-23). Ford and others (1993) explore the subject of radar image interpretation in depth.

The methodology for defining geological units and structural fabrics builds on standard geological analysis detailed in Wilhelms (1990) and Tanaka and others (1994), considering cautions of Hansen (2000), Zimbelman (2001), Skinner and Tanaka (2003), and McGill and Campbell (2004). Map units represent material emplaced within an increment of geological history, to which standard stratigraphic methods have some limited application; however, some units may be composite, because they might not be stratigraphically coherent over their

entire represented area and (or) they may have been emplaced over an extended period of time, particularly in relation to other units and (or) formation of secondary structures. Attempts are made to clearly separate secondary structures from material units; locations, orientations, and relative densities of primary and secondary structures are shown independent of material units. Further complicating the process of unraveling both temporal constraints and history, evidence for reactivation of secondary structures is common across the map area.

Criteria for distinguishing discrete geological units in the map area include (1) the presence of sharp, continuous contacts; (2) truncation of, or interaction with, underlying secondary structures and topography; and (3) primary structures, for example flow channels or edifice topography, that allow a reasonable geological interpretation and hint at three-dimensional geometry. Some mapped units fail to fit these constraints, limiting their use in constructing stratigraphic interpretations. Composite units, in particular, cannot provide robust temporal constraints, even of a relative nature.

Unlike surface crater statistics for planetary bodies that have old surfaces and high crater densities, such as the Moon and Mars, Venus impact crater statistics cannot place constraints on the age of surface units that cover the small areas visible in the map area (Hauck and others, 1998; Campbell, 1999). Age constraints may be established only where units are in mutual contact and (or) interact with the same suite of secondary structures. Such temporal constraints are only locally applicable and cannot be robustly extended across the map area.

Ranges of structures, both primary (depositional or emplacement-related) and secondary (tectonic), are identified in the Magellan SAR data. Primary structures include channels, shields, lobate flow fronts, and impact crater haloes and rims. Channels represent sinuous, low-backscatter troughs hundreds of kilometers long and a few kilometers wide; locally, they may lack apparent topographic relief (Baker and others, 1992, 1997). Shields are small (generally 1–15 km diameter; rarely 20 km diameter), quasi-circular to circular, radar-dark or radar-bright features with or without topographic expression and with or without a central pit (Guest and others, 1992). The size of individual shields is difficult to constrain because bases of individual shields are typically poorly defined, and deposits commonly blend smoothly into a composite layer that cannot be robustly treated as a time line or marker unit. Pits, sharply defined depressions, or pit chains, which are linear arrays of pits, likely represent regions marked by subsurface excavation and, as such, they may mark the surface expression of dilatational faults or dikes (Okobu and Martel, 1998; Bleamaster and Hansen, 2005; Ferrill and others, 2004; Schultz and others, 2004). Pits or pit chains can be considered primary structures or secondary structures, depending on the question at hand; pits are primary structures relative to pit-related materials, yet they may be secondary structures relative to the units they cut or are emplaced within.

Most radar lineaments represent secondary structures. Stofan and others (1993) provide an excellent introduction to the interpretation of secondary structures in Magellan SAR imagery. Extremely fine, sharply defined, continuous radar-bright lineaments, typically occurring in the lowlands, have commonly been interpreted as fractures (Banerdt and Sammis,

1992; Banerdt and others, 1997). If a fracture is associated with pits, it may represent the surface expression of a subsurface dike or a dilatational fault. Paired parallel dark and light lineaments that are separated by more than a few kilometers and describe linear troughs are generally interpreted as graben.

In SAR imagery, the opposite of a groove (linear trough) is a ridge (positive linear topography marked by parallel light and dark lineaments with the light lineament closest to illumination direction). On Venus, ridges typically have either parallel edges with moderate sinuosity at the 10-km scale and an across-strike gradation in backscatter (a form specifically called ridges in this text), or they have a more erratic plan view with common high-angle interruptions at the 10-km scale and variations in across-strike width (wrinkle ridges). Warps consist of positive linear topographic features, on the order of a hundred kilometers across and as much as thousands of kilometers long; warps, which are too subtle to appear prominently in SAR data, are discernible in topographic data.

Parallel bright and dark lineaments that form a fabric marked by alternating parallel ridges and troughs and have typical wavelengths of 2–5 km are called ribbons, ribbon fabric, or ribbon terrain (fig. 3, map sheet; Hansen and Willis, 1996, 1998). Bindschadler and others (1992a) called ribbons “narrow troughs.” Ribbon fabrics are commonly spatially associated with folds; fold crests typically trend at a high angle (generally 90°) to the ribbon lineaments. Graben, also commonly spatially associated with ribbons, typically parallel ribbon trends, but they can be differentiated from ribbons based on smaller length:width ratios. Graben that occur within ribbon terrain typically cut across fold crests, resulting in a lens-shape plan view. Collectively referred to as ribbon-tessera terrain, or ribbon terrain for short, this distinctive composite tectonic fabric commonly marks tessera terrain. The composite fabric may reflect a progressive increase in the depth to the rheological brittle-ductile transition with time and fabric development (Hansen and Willis, 1998; Ghent and Hansen, 1999; Brown and Grimm, 1999). For a discussion of ribbon-terrain controversies, see Gilmore and others (1998) and Hansen and others (2000).

Terminology

Clarification of the terminology used to describe and discuss Niobe Planitia quadrangle (V-23) is necessary, because terminology often carries stated and unstated assumptions regarding genetic implications or resulting from individual experience.

The term “lowland” is used in a topographic sense to describe broad regional long-wavelength (>100s of kilometers across) basins. The term “planitia/planitiae” refers to individual geomorphic basins or lowland regions. The general term “plains” describes geologic units only when the referenced published work uses that term.

The term “terrain” describes a texturally defined region, for example, a region where tectonism imparted a surface with a penetrative deformation that disallows interpretation of the original unit or units (Wilhelms, 1990). Characteristic texture could imply a shared history, such as a terrestrial tectonothermal history or an event that melds possibly previously unrelated

rock units (any combination of igneous, metamorphic, and sedimentary rocks) into gneissic terrain; no unique history is inferred or required prior to the event(s) that melded potentially separate units into the textural terrain. Events prior to terrain formation are unconstrained in time or process unless specifically noted. Examples of terrain in the map area include ribbon-tessera terrain (also called ribbon terrain), fracture terrain, and shield terrain.

Eruptive centers are called “shields” (terminology from Guest and others, 1992). An area where shields and associated eruptive materials appear to coalesce into a thin, regionally extensive layer is called “shield terrain”. Shield terrain is a composite unit terrain that consists of tens of thousands of individual shields and coalesced flow material, referred to as “shield-paint” for its apparent low viscosity (like liquid paint) during emplacement (Hansen, 2005). Shield paint, which acquires post-emplacement mechanical strength (like dry paint), could be formed from any combination of lava flows, air-fall deposits, or pyroclastic flows (Guest and others, 1992). Note that flooding by this radar-smooth flow material highlights gently sloping topographic features that would not normally be visible in Magellan SAR data. Shield terrain contains rocks with an interpreted shared emplacement mechanism (represented by primary structures), which differs from ribbon and fracture terrains that contain rocks with an interpreted shared deformation history (represented by secondary structures). Absolute time involved in terrain formation is completely unconstrained. Shield terrain in the map area includes edifices (shields) and associated deposits (shield paint).

The term “inversion structure” is used to record a sequence of geologic events, which could be genetically related or unrelated; the nature and relative order of the events, rather than the genetic relation between events, are critical to inversion structure formation. Initial formation of extensional fractures results in linear negative topography called “fracture troughs,” which are subsequently filled by a thin layer of surface material (DeShon and others, 2000). Later contraction causes inversion of the trough fill, resulting in the formation of linear structural ridges, or inversion structures, parallel to host fractures.

Geologic Setting

The vast lowlands display an extensive suite of generally north-striking fractures and a suite of east-northeast to east-trending wrinkle ridges. These lowlands also host tens of thousands of individual shields. The shields and associated eruptive materials coalesce into a thin, regionally extensive shield terrain layer that forms a regionally thin, locally absent veneer across much of the lowlands. Shield terrain is locally deformed by (predates) and locally masks (postdates) secondary structures including regional fractures and wrinkle ridges. In general, wrinkle ridges concentrate where shield terrain is presumed slightly thicker than average, and fractures dominate at the surface where shield terrain is presumed slightly thinner or absent.

Isolated kipukas of ribbon-tessera terrain (Hansen and Willis, 1998) locally protrude through the shield-terrain veneer, preserving evidence of local surface processes that predated

shield-terrain emplacement, as well as providing evidence for the extensive regional development of tessera-terrain fabrics. Ribbon-tessera fabrics are similar to the fabrics that characterize high-standing crustal plateaus, such as nearby Ovda and Thetis (V-35 and V-36) Regiones. Ribbon-bearing kipukas may preserve evidence of ancient collapsed crustal plateaus (Phillips and Hansen, 1994; Ivanov and Head, 1996; Hansen and Willis, 1998; Ghent and Tibuleac, 2002), or they may record different, but rheologically similar, processes. Ribbon terrain and associated shield terrain extend eastward into V-24 and northward into V-11 and V-12, where shield terrain was first recognized as an areally extensive geologic unit (Aubele, 1996).

Geologic Relations

The Niobe Planitia quadrangle lies along the north edge of Aphrodite Terra, where it preserves a transition from southern highlands to northern lowlands. Mesolands (the intermediate topographic level of Venus), as a topographic province, are essentially absent or represented only by Gegute Tessera.

Ovda Regio and Haastse-baad-Gegute Tesserae also display intratessera basin material (*itbO* and *itbHG*, respectively) and marginal intratessera flow material (*fitm*). The Niobe Planitia fracture terrain (*frN*) occurs as isolated kipukas, in locally elevated regions such as rims of coronae, and within the cores or interior highs of dorsa, as well as scattered outcrops across the map area. Neither the host unit nor the fractures likely record temporally distinct events. The host is likely a composite unit; the fractures commonly parallel the outcrop pattern of unit *frN* and may have formed synchronously with local basal terrain modification. Although the two styles of basal terrains occur across the map area, unit *rtu* dominates the eastern lowland, whereas unit *frN* dominates the western lowland. These basal terrains are variably covered with an apparently thin veneer of material called shield terrain. Shield-terrain material (*S*) is marked by extensively distributed small (~1–10 km diameter) shield edifices and associated local deposits (Hansen, 2005). Unelanuhi Dorsa (~100 km wide and over 2,000 km long), trends northwest parallel to the northeast boundary of Ovda Regio and extends into V-22 to the west; basal terrain resides within its core. The vast lowland within the map area displays an extensive suite of generally north-striking fractures and a suite of east-northeast- to east-trending wrinkle ridges, which variably cut units *frN* and *S*. The lowland also includes localized deposits (smooth flows, undivided, unit *fsu*) marked by relatively smooth radar character. This unit is interpreted as relatively radar smooth flows that may represent a mixture of both geologic and radar units.

The lowlands also host five coronae, each marked by subdued or basin-like topography: Dhisana, Allatu, Omeciuatl, and Bhumiya Coronae cluster loosely in the east-central map area and Maya Corona occurs in the northwest (lat 23° N., long 97° E.). Rosmerita Corona (outside of V-23) spawns flows (unit *fcR*) that spilled across topographic lows within Haastse-baad Tessera. The five coronae within the map area display no obvious flow units that can be uniquely attributed to these features at map scale; each feature is marked by topographic and structural

elements as discussed in the sections on tectonic structures and coronae. A volcanic structure, marked by a flat-topped edifice and radial flows (units *fEa* and *fEb*), occurs in the northwest corner of the map area.

Basal Terrain Units

Basal units in the Niobe Planitia quadrangle (V-23) are commonly associated with local highs (100s of meters high, generally >10 km across); but not all basal units correlate with local highs and not all local highs correlate with the exposure of basal units. The basal units form two packages differentiated by structural character: ribbon-tessera/intratessera and fracture terrains. Ribbon-tessera terrain characterizes the highland, occurs in large tracts across Ovda Regio (*rtO*) and Haastse-baad and Gegute Tesserae (*rtHG*), and occurs in lowland kipukas across much of map area (*rtu*).

Tessera and Intratessera terrain

Tessera terrain within the map area includes ribbon-tessera terrain of Ovda Regio (unit *rtO*), ribbon-tessera terrain of Haastse-baad and Gegute Tesserae (unit *rtHG*), and undivided ribbon-tessera terrain (unit *rtu*). Each tessera-terrain unit hosts ribbon structures (Hansen and Willis, 1998) and commonly hosts fold ridges. In general, ribbons and folds trend perpendicular to one another, although tectonic fabric character in unit *rtu* is more difficult to delineate with confidence.

A composite tectonic fabric comprised of folds, ribbons, and complex graben characterizes ribbon-tessera terrain (fig. 3, map sheet). This fabric, which varies in detail from location to location, is characterized by (1) relative orientation of ribbons, folds, and complex graben, (2) relative spacing of structural suites, and (3) the penetrative development of the composite fabric relative to the scale of image resolution. Ribbon structures generally trend perpendicular to fold crests, as do late graben (Bindschadler and Head, 1991; Hansen and Willis, 1998, 1996; Pritchard and others, 1997; Brown and Grimm, 1999; Ghent and Hansen, 1999). At many locations, three or more distinct fold wavelengths are visible in altimetry data (Hansen, 2006): approximately 0.5 to 2–5 km, 10 to 15 km, and very long wavelengths of 30 to 100 km. Short- and medium-wavelength folds occur within the troughs, limbs, and crests of longer-wavelength folds. Short-wavelength folds locally curve across longer-wavelength fold crests with angles generally greater than 30°. Low viscosity material (lava?) locally fills troughs of short-, medium-, and long-wavelength folds. Flooded short-wavelength fold troughs occur along long-wavelength fold troughs, limbs, and crests. Locally filled basins occur at a range of scales from the troughs of short-wavelength folds and extensional structures to intratessera basins (Banks and Hansen, 2000) visible at map scale (fig. 4, map sheet).

Large intratessera basins (Bindschadler and Head, 1991; Banks and Hansen, 2000) that contain radar-smooth fill generally trend parallel to the fold troughs. Intratessera basin material, generally radar smooth in character, is defined as two separate map units, intratessera basin material of Ovda Regio tessera terrain (unit *itbO*) and intratessera basin material of

Haastse-baad and Gegute Tesseræ terrain (unit *itbHG*), based on location and host tesseræ terrain. Relatively large regions of these units are visible at map scale, although they are also visible at smaller scales (figs. 3, 4, map sheet). Locally, short, closely spaced extensional structures cut orthogonally across short-wavelength fold crests, typically with little to no indication that these same structures cut long-wavelength fold crests, indicating that both early layer contraction and early layer extension contributed to ribbon-terrain-fabric formation. Ribbon structures are commonly deformed by medium- to long-wavelength folds, indicating relative early ribbon formation (Hansen and Willis, 1998), but short wavelength fold fabrics are clearly truncated by short to medium extensional structures, indicating that layer contraction and extension occurred throughout ribbon-terrain evolution. Widely spaced extension structures form complex graben locally; complex graben cut all folds that form late in the evolution of ribbon-terrain fabric (Bindschadler and others, 1992a; Gilmore and others, 1997; Hansen and Willis, 1996; 1998; Brown and Grimm, 1999; Ghent and Hansen, 1999).

Ribbon-tesseræ-terrain units (*rtO*, *rtHG*, *rtu*) range topographically from highest to lowest instead of stratigraphically, because relative temporal relations are unconstrained. Unit *rtO*, confined to the southwestern part of the map area, represents the northeastern part of Ovda Regio and extends into adjacent V-22, V-34, and V-35 quadrangles. Unit *rtHG*, which crops out in the southeastern and eastern parts of the map area, extends eastward into V-24 and southward into V-35. Unit *rtu* occurs as isolated kipukas across the eastern and central map area.

Ribbon-fold fabrics in unit *rtO* describe a coherent pattern. Folds trend northwest parallel to the local northwest margin of Ovda Regio, curving to a more northward trend toward the east and into V-35 to the south (Bleamaster and Hansen, 2005). Ribbon structures generally trend perpendicular to fold crests, as do late graben. Intratessera basins with radar-smooth fill generally trend parallel to the fold troughs. In the southwestern map area, the structural fabrics preserved in unit *rtO* and the intratessera basin fill (intratessera terrain volcanic material of Ovda Regio, unit *itbO*) describe more complex patterns: folds trend north with local sinuous traces; ribbons trend north-northeast and northwest; and aerially extensive intratessera basins comprise two general trends, parallel to northwest-trending fold troughs in the northeast and parallel to north-trending folds in the south.

Elevation and structural fabric patterns delineate unit *rtHG* from unit *rtO*. Whereas unit *rtO* generally lies above 6,054 km elevation, unit *rtHG* lies within the range 6,051.5 to 6,053.5 km with lower elevations to the north. Near the boundary between Haastse-baad and Gegute Tesseræ to the east and Ovda Regio to the west, folds and intratessera basin fill (unit *itbHG*) in unit *rtHG* trend northeast and ribbons trend northwest perpendicular to fold crests. To the north within Haastse-baad and Gegute Tesseræ, fold crests and intratessera basins also trend northeast. Ribbon fabrics trend perpendicular to the fold crests, but short-wavelength folds parallel the fold crests. At least some of the northwest-trending lineaments appear to be ribbon ridges and troughs, although, locally, some may be short-wavelength folds. Data resolution does not allow confident structure identification in each case. Within the region between the northeast- and

northwest-trending intratessera basins, some basins display possible hybrid orientations and patterns. Detailed geologic and structural mapping of the intratessera basins is outside the scope of this study, although construction of such maps would likely provide clues to basin formation in relation to the structural evolution of the hosting tesseræ terrain. Although Haastse-baad and Gegute Tesseræ define separate geographic locations, they provide no clear geological character that distinguishes the two regions; hence, they are considered a single geological unit. As noted, terrain elevation and the occurrence of intratessera basins decrease to the north, which could relate to overall elevation and the related ability to delineate intratessera basins.

Ribbon-tesseræ terrain, undivided (unit *rtu*), occurs in numerous kipukas across the central, northern, and eastern map area. The highly irregular boundaries of unit *rtu* reflect the detailed structural topography that results from the composite ribbon-fold fabric and the interaction of this topography with younger overlying deposits. Isolated kipukas of unit *rtu* show gradational contacts with overlying material; many exposures of unit *rtu* exist well below the 1:5,000,000 map scale. Each kipuka of unit *rtu* preserves a penetrative fabric, consisting of one or two lineament trends; the fabric defines the kipuka material as tesseræ terrain. In some kipukas, the lineaments can be distinguished as ribbons or as fold crests; in other kipukas, lineament trend, but not character, can be determined. Lineaments among all of the *rtu* kipuka—no matter how small or how widely separated—show parallel trends. These trends also parallel the fabric trends that are preserved in and that characterize unit *rtHG*. Although spatial relations and relative ages among the *rtu* kipukas cannot be uniquely defined, the parallelism of penetrative fabrics is consistent with the interpretation that unit *rtu* forms a continuous subsurface unit and that the kipukas preserve synchronously formed terrain, recording a common history. The similar character and parallelism of fabrics in units *rtu* and *rtHG* might reflect a shared history of these two spatially separate units, as well; this interpretation is consistent with, but not required by, the current data. However, tectonic fabric patterns preserved in tesseræ terrain associated with Ovda Regio and with Haastse-baad and Gegute Tesseræ and in tesseræ terrain inliers describe different regional strain patterns consistent with, but not required by, the interpretation that these two tracts of tesseræ-terrain (*rtO*, *rtHG*) formed as separate morphological features (Bindschadler and Parmentier, 1990; Bindschadler and others, 1992b; Bindschadler, 1995; Phillips and Hansen, 1994, 1998; Hansen and Willis, 1998; Hansen and others, 1999, 2000).

Marginal intratessera terrain flow material (unit *fitm*), characterized by radar-smooth material, fills local lows within the associated ribbon terrain along the margins of Ovda Regio crustal plateau. Unit *fitm* does not have any clear, internal, crustal-plateau sources and occurs marginally along Ovda Regio. These flows locally host structures that resemble ribbons and folds. However, unit *fitm* blankets the structures; thus, tesseræ structures may have been reactivated to deform unit *fitm*, which suggests that unit *fitm* dominantly postdated the formation of tesseræ fabrics. Timing between the formation of units *itbO* and *fitm* is difficult to determine, and the relative order of emplacement may vary from location to location. Unit *fitm* flows may be attributed to similar emplacement processes as unit *itbO* and

simply show a different surface morphology due to flow thickness and depositional environment, or they may be unrelated.

Fracture Terrain

Kipukas preserved mostly in the northwestern part of the map area host another basal unit, Niobe Planitia fracture terrain (unit frN). Kipukas of unit frN show sharp to diffuse, but extremely detailed, contacts and appear locally buried or partially obscured by surface material, shield-terrain deposits (unit S). Unit frN hosts generally north-striking fractures where exposed, but individual exposures also show fracture patterns that correspond to local topography, likely indicating that the terrain records both a shared history of modest easterly directed extensional strain, as well as localized low strain deformation related to topographic warping. The relative age among individual kipukas is not constrained, nor is the relative timing of surface material that crops out at some distance from the terrain-bearing kipukas. At the location of the contact, shield terrain clearly postdates development of the tectonic fabric and, therefore, postdates the host material as well. Strain fabrics recorded in the kipukas could have formed in a spatially localized fashion, which explain many exposures of unit frN where the fracture pattern mimics the local topography.

Shield Terrain Material

Shield terrain (unit S) is the most aerially extensive terrain across the map area. Individual shields are radar-dark or radar-bright, quasi-circular to circular features (flat-topped or flat shield, dome, cone) with or without a central pit (fig. 5, map sheet). Embayment relations indicate that flows spread across the surface into local topographic lows and around local topographic highs, coalescing with material from adjacent edifices to form a thin layer of shield paint (fig. 6, map sheet). Shield paint forms a thin, regionally extensive but locally discontinuous layer that appears lacelike and locally hides and thinly veils stratigraphically lower unit frN and (or) ribbon-tessera-terrain units (fig. 7, map sheet). The scale of lacey holes in the shield-paint veil ranges from tens to hundreds of square kilometers. The lacey holes suggest that shield paint probably flowed across the surface, rather than being emplaced as an air-fall layer, which would form a more continuous blanket. Shield paint hosts spaced fractures, wrinkle ridges, and inversion structures that indicate the acquisition of some inherent mechanical strength following unit emplacement.

The smallest size of individual shield edifices is difficult to determine because many pixels are needed to image a single shield; thus, although full-resolution Magellan SAR data has approximately 100 m/pixel resolution, the effective resolution for shield size is likely approximately 0.5 to 1 km diameter (Zimelman, 2001; Guest and others, 1992). Minimum discernable shield diameter depends on size, morphology, radar incidence angle, radar contrast with surroundings, texture of surroundings, and character and number of adjacent shields. Because approximately 0.5- to 1-km-diameter shields can be identified locally in the map area, it is likely that even smaller shields also exist. Guest and others (1992) reached a similar

conclusion. In addition, shield size is difficult to constrain because shield bases are commonly poorly defined; individual edifices typically appear to blend smoothly into a base layer of coalesced shield paint. In some places, a slight difference in radar backscatter or truncation of pre-existing underlying structural fabric can define the apparent limit of individual shields, or it might mark a change in thickness of shield paint. Figure 5 illustrates a range of shield morphologies: (1) aprons that blend outward into surrounding terrain, (2) edifices that are distinct from surroundings, (3) edifice morphologies that range from steep to broad and from cone shaped to flat topped, and (4) extremely flat regions that contain low-viscosity material that flowed into subtle topographic lows.

The density of shields is also difficult to determine because shield identification depends on image resolution, as well as the experience of the geologist. In the map area, shields were ranked by confidence levels (table 1): definite shields (obvious shields) and potential shields (possibly controversial features). The major distinction between these divisions relates to data resolution and geologists' experience. Shields likely exist below SAR resolution, making maximum estimates difficult to determine. Minimum estimates of definite-shield densities range from 3,550–10,500 shields/10⁶ km². Combined (both definite and potential) shield densities range from 15,650–33,675 shields/10⁶ km²; these values are neither minimum nor maximum values, simply estimates.

No direct correlation exists between the number of definite and combined shields in the map area: the area centered at lat 23° N., long 103° E. (fig. 6A) hosts the fewest combined shields, yet the most definite shields and the area centered at lat 13° N., long 111° E. (fig. 8A, map sheet) has the fewest definite shields and the most combined shields. The average number of definite shields (247) and combined shields (938), representing average total densities of approximately 6,255 and approximately 23,445 shields/10⁶ km², respectively, are slightly greater than, but similar to, the shield plains of Aubele (1996; 4,500 shields/10⁶ km²).

Figures 6–10 (map sheet) show details of five 2°x2° images from the map area that illustrate shield patterns, densities, relations with basal-terrain units, and secondary structures. Each area (1) has both right- and left-illumination SAR images that lack large data gaps; (2) lacks large impact craters, large tracts of ribbon terrain, or extensive basal fracture terrain, all of which could hamper shield identification and interrupt shield patterns; (3) hosts regional easterly trending wrinkle ridges and northerly striking fractures; and (4) yields clues for shield-terrain formation. Areas shown in figures 6–10 are named for their location, for example figure 6, centered at lat 23° N., long 103° E. is referred to as 23N/103E.

23N/103E

Area 23N/103E (fig. 6A) contains a similar distribution of definite shields (402) and combined shields (754). An approximately 20 km wide data gap obscures the north-central part of the map area. Temporal relations between shields and wrinkle ridges are difficult to determine robustly because these primary and secondary structures have relatively small size and spacing and the shields or variations in shield-paint thickness could

contribute to strain partitioning during wrinkle-ridge formation. Locally, a shield appears to truncate a wrinkle ridge along trend and, therefore, would postdate wrinkle-ridge formation. It is also possible that the shield was emplaced prior to wrinkle-ridge formation, and ridge formation ended as it approached the shield representing an area of greater layer thickness and, hence, strength. In addition, the large number of individual shields and individual wrinkle ridges may infer that wrinkle-ridge and shield formation were partly penecontemporaneous.

In the region between wrinkle ridges, polygonal wrinkle-ridge structure is best developed away from shield centers, indicating that the polygonal structures most likely formed after individual shields. The pattern likely reflects strain partitioning resulting from a thicker material layer near shield centers. But early polygonal fabric formation is also possible, which suggests that the subsequent thin shield flows cover the pre-existing ridges. The polygonal fabric shows either a preferred longitudinal shape parallel to the trend of the wrinkle ridges or no preferred shape.

In the southeastern part of the image, shields are superposed on a locally preserved basal layer cut by closely spaced, east-trending, anastomosing lineaments (fig. 6D). The patch-like outcrop pattern of these kipukas of basal terrain, which are not visible at map scale, indicates the extremely thin nature of the overlying shield terrain unit. The penetrative fabric is discussed further in the section on regional structures.

Locally, north-northwest-striking fractures cut the shield paint, but the discontinuous nature of many fracture traces suggests that these fractures were locally reactivated and original fractures likely predated most shield paint. These relations are also consistent with a thin shield-terrain layer.

21N/113E

Area 21N/113E (fig. 7A), which hosts almost an order of magnitude more combined shields (1,080) than definite shields (167), shows similar relations between wrinkle ridges and fractures. This region also preserves patches of extremely fine scale polygonal fabric that has diffuse to relatively sharp boundaries (fig. 7C). Both definite and potential shields occur within the region defined by fine polygonal fabric without obvious flow boundaries. Potential shields are more prominent in the region deformed by polygonal fabric, which may simply reflect a contrast with a subtly textured substrate. Mottled areas free of small-scale polygonal fabric could be aggregates of subresolution shields. Wrinkle ridges cut the polygonal fabric boundary with no obvious spatial pattern relative to the fine polygonal fabric, indicating that there is likely a relative mechanical coherence in the layer across this boundary, although layer thickness may differ across the boundary. The region between wrinkle ridges preserves a fine-scale polygonal fabric that appears to grade in scale across the enlarged image (fig. 7A). Northerly striking fractures parallel to the regional trend are covered by shield paint, yet fractures locally cut individual shield edifices. The fractures show a spatial correlation with the areas of smaller-scale polygonal fabric. Both observations are consistent with the interpretation that the shield terrain layer is thinner in the area of small-scale polygonal fabrics. An approximately 15

km diameter circular depression marks the northeast corner of 21N/113E; extremely fine, commonly covered fractures concentric to this structure extend 60–70 km from its center.

13N/111E

Area 13N/111E (fig. 8), located in Sogolon Planitia, also shows an order of magnitude more combined shields (1,340) than definite shields (140), east-trending wrinkle ridges and north-striking fractures. Locally, shields postdate formation of north-trending lineaments that both cut and invert shield-paint material (fig. 8C). The lineaments are apparently extension fractures, in places filled with shield-paint material, which was subsequently shortened, resulting in formation of inversion structures (DeShon and others, 2000). Fracture fill (shield paint) was apparently extremely localized and deposited as a thin, lace-like layer, indicated by (1) open fractures transitioning into inversion structures along strike and (2) the close spatial location of open fractures and inversion structures.

23N/117E

Area 23N/117E (fig. 9A) hosts four times as many combined shields (1,000) as definite shields (250), as well as inversion structures. In the northeast corner of this area, kipukas of ribbon-tessera terrain peek through a veil of shield terrain. Shield paint embays the detailed ribbon-terrain topography, comprised of alternating, parallel, north-trending ridges and troughs. Shield paint blends into a coherent layer; shields are locally visible due to topographic expression. Isolated patches of fine-scale polygonal fabric occur locally (fig. 9D) and gradually increase in spacing away from the shields, which is consistent with an interpretation that shield paint is thicker near the edifices. Locally a secondary structural fabric, marked by delicate, closely spaced (~500 m or less), short (~5–20 km), northeast-trending lineaments (fractures?), transects the surface discontinuously (fig. 9E). The fabric is visible in patches that have a parallel lineament trend and similar lineament spacing. Fabric continuity across spatially separate regions supports the interpretation that this fabric is secondary. The tight lineament spacing likely reflects deformation of a thin layer, interpreted as shield paint in this image. Similar subtle lineament fabrics (with various orientations) across much of the Niobe Planitia map area are not visible at map scale.

13N/119E

Area 13N/119E (fig. 10A) includes ribbon-terrain kipukas, wrinkle ridges, fractures, and definite (270) and combined (630) shields. Ribbon terrain shows relatively high relief, rising from several hundred meters along the northern edge of the image. Ribbon trends parallel those preserved in isolated kipukas across the map area. Shields and shield paint occur across the topographic range of ribbon terrain, forming high, isolated deposits (fig. 10C). Even at high elevation, shield paint that flowed into localized lows gently masks ribbon fabrics, indicating that (1) shield terrain postdates ribbon-terrain formation, (2) shield terrain lies directly above ribbon terrain, (3) shield terrain forms discontinuously across local high relief (that is, it cannot

be connected by a continuous datum indicative of low-elevation embayment), and (4) shield paint is locally very thin. Regional continuity of ribbon trends between kipukas is consistent with the interpretation that ribbon terrain extends beneath shield paint across much of the map area and that shield terrain is thin at both a local and a regional scale. Delicate wrinkle ridges that cut shield paint east of the ribbon-terrain kipukas parallel regional trends. North-striking fractures both cut and are covered by shield paint, indicating that at least a part of the activity on these structures (likely reactivation) was pencontemporaneous with shield-terrain formation.

Several independent observations indicate that shield terrain forms a thin veneer, both locally and regionally: (1) extremely complex contacts between shield terrain (unit **S**) and underlying basal terrains across the central and northern map area, marked by low topographic relief; (2) detailed contacts between shield terrain and underlying units; (3) lace-like character of shield terrain; (4) local fracture filling of shield terrain and subsequent structural inversion with changes along strike from fracture trough (unfilled) to inversion structures; (5) occurrence of fine-scale polygonal fabric on shield terrain; (6) widespread reactivation of subterrain fractures; and (7) the occurrence of numerous small kipuka of ribbon terrain across huge expanses of very low topographic relief. Guest and others (1992) estimated that shield deposits are likely tens of meters or less in thickness. Robust quantification of layer thickness is difficult using available SAR data, but layers tens of meters thick or less are consistent with observations 1–7.

Flow Units

Flows originating within V–23

Smooth flows, undivided (unit **fsu**), occur in the southwest lowland region just north of Ovda Regio. This unit is interpreted as radar-smooth flows that may represent a mixture of both geologic and radar units. Unit **fsu** typically lies in contact with unit **s** (shield terrain), although locally it abuts unit **rtu** (ribbon-tessera terrain). The contact between units **fsu** and **s** is typically gradational. Shield edifices lie within the mapped limits of unit **fsu**, and unit **fsu** likely locally embays unit **s**. Units **s** and **fsu** are interpreted as mutually time transgressive. In some places, unit **fsu** postdates the emplacement of locally defined unit **s**, as evidenced by the burial of wrinkle ridge structures that deform and, therefore, postdate local occurrences of unit **s** (lat 11° N., long 96° E.).

In the northwest corner of the map area, Ezili Tholis (~100 km diameter, as high as 6,053.5 km) perches above the surrounding lowland. Two suites of associated flows, units **fEa** and **fEb**, are distinguished on the basis of SAR and altimetry data. Each unit comprises numerous intermediate- to high-radar-backscatter lobate flows that radiate outward from the topographic edifice. Unit **fEb** flows are proximal to the summit; are marked by higher-radar backscatter, likely indicating a rougher surface; and occur along a steep slope. Unit **fEb** may be younger than unit **fEa**, but relative timing between the two units is unconstrained. Unit **fEa** distal flows extend outward from the volcano as far as 200 km. The flows were affected by local

topography, where they are buttressed to the east by a local high extending above 6,052 km and are decorated with basal terrain (Niobe Planitia fracture terrain, unit **frN**). Local high areas, as high as 6,052.5 km, also deflect unit **fEa** flows to the south; a local high along the quadrangle boundary (lat 22.5° N., long 90° E.) splits local flows. Kipukas of unit **frN** are surrounded by unit **fEa**. Wrinkle ridges cut units **fEa** and **fEb**, which also contain small shield edifices.

The five coronae within the map area display no obvious flow units that can be identified at map scale.

Rosmerta flows

Rosmerta Corona is a 300-km-diameter, radial, domical corona that lies outside of the map area along the boundary between V–24 and V–36 (centered at lat 0° N., long 124.5° E.; Thetis Regio quadrangle). In the southeastern map area, flows that emanate from Rosmerta Corona flow northwest and fill local topographic basins within Haastse-baad Tessera (unit **rtHG**). Rosmerta Corona flow material (unit **fcR**) shows mottled to radar-smooth character and can be traced to the central region of Rosmerta Corona. Some of the material mapped as Haastse-baad and Gegute Tessera intratessera basin fill (unit **itbHG**) may have originated from Rosmerta Corona, having been connected with unit **fcR** either through narrow surface passages in the tessera-terrain fabric that are not visible at map scale or through the subsurface. Both unit **fcR** and unit **itbHG** show local shield edifices.

Impact Features

At least 24 impact craters, ranging from 3 to 63 km in diameter, dot the map area (table 2). Essentially all of the impact craters show ejecta blankets, whereas only three show clear halo deposits; 17 craters have radar-smooth interiors, interpreted as interior fill. Crater densities for individual craters range from 1.91 to 3.82 craters/10⁶ km², with an average crater density of 2.97 (Herrick and others, 1997). Half of the craters have densities >3.0 craters/10⁶ km² and seven craters have densities >3.5 craters/10⁶ km², which is higher than the Venus global average (~2 craters/10⁶ km²; Phillips and Izenberg, 1995; McKinnon and others, 1997). Although there are too few craters to constrain the ages of individual surfaces on Venus (Hauck and others, 1998; Campbell, 1999), the relatively high crater density and the paucity of crater haloes may indicate that the map area represents a relatively old composite surface that is mostly older than the Venusian average model surface age (Phillips and Izenberg, 1995; Hansen and Young, 2007).

None of the impact craters formed during a unique event; therefore, the crater units represent clear diachronous unit emplacement. Unit **cu** (crater material, undivided) represents ejecta deposits associated with local, time-transgressive bolide impact. Some impact-crater interiors include a radar-smooth material that is also mapped as unit **cu**. Two additional impact-crater-related units appear spatially associated with Ferrier crater. Units **coa** and **cob** are interpreted as radar-rough and radar-smooth outflow facies, respectively. Unit **coa**, which is proximal to Ferrier crater, displays a heterogeneous texture;

whereas, unit COB, the distal facies, is relatively radar smooth. Both units appear to locally bury wrinkle ridge structures that deform locally preserved shield terrain (unit S). Thus, units COA and COB, and Ferrier Crater by association, appear to have formed after the formation of local wrinkle ridges. In general, units COA and COB cover north-striking fractures, as evidenced by the general truncation of fractures in spatial correlation with the limits of units COA and COB. However, locally, units COA and COB are cut by north-striking fractures, which is likely the result of local structural reactivation.

Tectonic Structures

Both local and regional tectonic structures occur across Niobe Planitia quadrangle (V-23). Local structural patterns are generally areally confined or associated with individual features, such as coronae; whereas, regional structures describe coherent patterns across a much larger area. The timing of local structures likely corresponds to the formation, or stages of formation, of the individual features with which they are associated. Temporal evolution of regional tectonic structures is more difficult to constrain, may be time transgressive, and (or) involve reactivation.

Regional structural suites

Regional structures in the map area include four types of tectonic structural suites: (1) ribbon-tessera fabrics, (2) extensional fractures, (3) wrinkle ridges, and (4) inversion structures. Ribbon-tessera fabrics are described above in the section called Tessera and Tessera Terrain.

Regional Extensional Fractures

Regional extensional fractures, which generally strike north-northwest, display coherent tectonic patterns across the northern two thirds of the map area. These lineaments are interpreted as extensional fractures on the basis of their straight, sharp character and lack of notable topographic expression, or along strike offset. Fractures shown on the geologic map indicate the general trend and character of the fracture suite, however fracture spacing, 1–2 km or less (locally down to the resolution of the current SAR data set), is too detailed to show on the 1:5,000,000-scale map. Extension fractures, best preserved in local topographic highs across the lowland, are both locally covered by, and cut, shield terrain material, indicating that the fractures were formed and (or) reactivated through time. Although the fractures generally describe a northerly trend, locally, fractures mimic local topography, indicating that some fractures formed (or were reactivated) during local uplift along topographic warps.

Wrinkle Ridges

Wrinkle ridges (figs. 6–10) define low sinuous ridges a few kilometers wide and as much as a few hundred kilometers long that are found on most terrestrial worlds, especially on

large flat expanses of volcanic flows (Watters, 1988). Wrinkle ridges, which trend east-northeast, occur across much of the northern two thirds of the map area as previously noted (Bilotti and Suppe, 1999). In Sogolon Planitia, wrinkle ridges trend northeast to locally northward, parallel to (1) northward striking fractures, (2) the Sogolon Planitia-Haastse-baad Tessera boundary, and (3) northeast to north-trending warps and ridges within Sogolon Planitia. North-trending Sogolon wrinkle ridges likely represent inversion structures, described in more detail below. Like the fractures, wrinkle ridges occur at a range of spacing, down to small-scale wrinkle ridges too closely spaced to show on the 1:5,000,000-scale geologic map. Locally, wrinkle ridges define fine-scale polygonal fabrics (fig. 7) much too small to show on the 1:5,000,000-scale geologic map. However, closely spaced wrinkle ridges parallel the trends shown on the geologic map. Small-scale wrinkle ridges wrap around individual shields, indicating that wrinkle ridges deformed a thin mechanical layer, very low-angle fault elements participated in the formation of these wrinkle ridges, or both. Wrinkle ridges locally deform shields but are also covered by shields, indicating diachronous formation of both shields and wrinkle ridges (fig. 6). Wrinkle ridges are notably absent within exposures of ribbon-tessera terrain in high-resolution imagery (figs. 5, 6), although wrinkle ridges extend to the contact between tessera terrain and shield terrain. These relations suggest that ribbon-tessera terrain is not rheologically amenable to wrinkle ridge formation (it lacks a thin deformable layer); whereas, the thin shield terrain veneer readily forms wrinkle ridges. Thus, the presence or absence of wrinkle ridges in this case is likely related to rheological criteria rather than temporal considerations.

Inversion Structures

Inversion structures (Buchanan and Buchanan, 1995) within the map area generally occur as north-trending ridges. Although the inversion structures are too small to appear on the 1:5,000,000-scale geologic map, their occurrence provides critical clues to the nature of shield terrain. Inversion structures record a sequence of geologic events, which could be genetically related or unrelated; the nature and relative order of the events, rather than the genetic relation between events, are critical to inversion structure formation. Initial formation of extension fractures results in linear negative topography. Fracture troughs are subsequently filled by a thin layer of surface material; later contraction causes inversion of the trough fill, resulting in the formation of linear structural ridges parallel to host fractures. Inversion structures noted elsewhere on Venus (DeShon and others, 2000) follow a similar sequence of events. In the map area, northerly trending fracture troughs were locally filled with shield terrain material and later shortened, inverting the fill to form northerly trending ridges (figs. 7, 8).

Fabric anisotropy and implications for stress-strain relations

Extension fractures and wrinkle ridges are examples of regionally distributed strain fabrics, interpreted as parallel to

maximum principle shortening and extension, respectively. The orientations of strain fabrics on Venus are commonly interpreted as a reflection of principle stress directions during wrinkle ridge (or fracture) formation (Sandwell and others, 1997; Solomon and others, 1999; Anderson and Smrekar, 1999; Banerdt and others, 1997; McGill, 2004). Such an interpretation requires that the host material was originally homogeneous and isotropic. Across the map area this assumption might not be robust. Wrinkle ridges and inversion structures provide illustrative examples.

In figure 6, basal terrain, which displays a penetrative fabric (closely spaced at the scale of observation) marked by local east-trending lineaments, is exposed through the lace-like veil of shield terrain. The east-trending linear fabric parallels the trend of adjacent wrinkle ridges, and it is likely that the older anisotropic fabric strongly influenced the orientation of younger wrinkle ridges. The penetrative fabric clearly predated shield terrain formation, which in turn must have predated the formation of wrinkle ridges; therefore, the host crust was anisotropic prior to wrinkle ridge formation. To illustrate the importance of an existing anisotropy in stress-strain relations, consider a section of corrugated cardboard (fig. 11, map sheet). The corrugations, small wavelength folds, define a penetrative structural/mechanical fabric anisotropy. Application of a wide range of orientations of principle stress axes would each result in the same orientation of longer wavelength folds (strain); in each case the resulting fold axes would parallel the original corrugations. Thus, the resulting strain can be almost independent of principle stress orientation. The strength anisotropy is so marked that application of principle compressive stress parallel to the corrugations will likely not result in formation of any shortening fabric. Corrugations or other mechanical anisotropy can either increase the overall strength of the material in the direction of the anisotropy, greatly inhibiting the formation of strain structures, or weaken the strength parallel to the anisotropy, and thus, greatly influencing the orientation of younger strain features, almost independent of differential stress orientation. A similar relation exists for fractures and later formation of inversion structures. In this case, a wide range of possible orientations of principle stress axes results in structural inversion of fracture fill and the formation of ridges parallel to the original fractures. Original fracture orientation, rather than the paleostress field that accompanied shortening, is responsible for inversion structure orientation (Withjack and others, 1995, 1998).

Coronae

The map area hosts five coronae—all of which are probably old coronae (Chapman and Zimbelman, 1998), or circular lows (McDaniel and Hansen, 2005). Each of these coronae is marked by an amphitheater-like depression and by concentric fractures or faults that are spatially correlative with a circular ridge. In addition, each of these features lacks well-developed radial fractures and obvious large flows, features typical of many coronae (Stofan and others, 1992, 1997) and particularly associated with postulated young coronae (Chapman and

Zimbelman, 1998). Although the lack of large distinctive flows could be a function of relatively old age and resulting radar homogenization (Arvidson and others, 1992), it is also possible that these features simply never had large obvious flows. We refer to these features as circular lows to emphasize descriptive character, rather than to hypothesize genetic evolution. Each circular low is described briefly below.

Maya Corona

Maya Corona (200 km diameter; lat 23° N., long 98° E.), in northwestern V-23, represents a circular basin as much as 900 m deep (relief from ridge to basin floor), surrounded by a low incomplete ridge (best developed along the western margin) and a suite of concentric fractures. The concentric fracture zone is best preserved on the basin interior and basin walls, although locally concentric fractures occur in the surrounding lowlands. Shield terrain (unit S) variably covers the fracture zone; locally the fractures show evidence of structural reactivation following local shield emplacement. Regional north-northwest-striking fractures and northeast-trending wrinkle ridges variably cut and are cut by shield terrain material. Wrinkle ridges show a slight change in trend inward toward the Maya basin. Horner impact crater, which lies along the northwest interior wall of Maya basin, clearly postdates formation of Maya and likely postdates shield terrain and regional fracture and wrinkle ridge formation, although reactivation of these suites of structures cannot be dismissed. Maya lacks radial fractures, evidence of obvious flows, and any evidence of early domical development that might have accompanied corona formation. Maya basin and the concentric fracture suite formed synchronously and predated the formation of shield terrain and the formation of the fracture suite and wrinkle ridges.

Dhisana Corona

Dhisana Corona (~100 km diameter; lat 14.5° N., long 111.5° E.) displays a 300–400-m-deep pear-shaped basin surrounded by concentric fractures and (or) faults developed along the basin wall and within the surrounding lowlands. The concentric fracture zone is mostly developed on the basin interior and basin walls, although locally concentric fractures occur in the surrounding lowlands and are visible through a thin cover of shield terrain. Locally, the fractures show evidence of structural reactivation following emplacement of individual shields. The basin hosts a central bulge decorated by shields. Two partially collapsed pancake domes, adorned with shields, lie along the northwest boundary of the basin, clearly overprinting the concentric fracture zone. Shield material, unit S, locally covers parts of the basin wall and floor, as well as the surrounding lowland. Regional north-striking fractures cut, and are covered by, shield material. Wrinkle ridges, parallel to regional trends, extend across Dhisana and deform unit S. The local geologic history that emerges includes (1) formation of unit rtu; (2) basin formation accompanied by development of the concentric fracture/fault zone; (3) interior mound formation and, presumably, pancake dome development within the same

time slice; (4) shield terrain evolution, including formation of north-striking fractures and generally east-trending wrinkle ridges, all developing in a time-transgressive fashion, broadly overlapping in time and space. Dhisana notably lacks radial fractures, obvious flows, and evidence of early dome development.

Allatu Corona

Allatu Corona (150 km diameter; lat 15.5° N., long 114° E.) forms a circular basin 300–400 m deep, marked by an approximately 75-km-wide zone of concentric fractures/faults. The fracture zone, which is locally blanketed by discontinuous shield terrain material (unit **S**), is best preserved along the northwest and southeast basin walls, although locally concentric fractures occur in the surrounding lowland region. The fracture zone is completely covered along the southwest margin. A pancake dome covers the fracture zone along the west basin margin, yet concentric fractures of the same trend locally cut the dome, recording structural reactivation. Shield terrain material (unit **S**) variably covers the surrounding lowland, parts of the fracture zone, the basin interior, and an interior peak that lies off center in the northeast part of the basin. North-striking fractures cut and are covered by unit **S**. Wrinkle ridges, parallel to the regional trend, deform shield terrain material (unit **S**). The concentric fracture zone has a slight asymmetric form with a narrower footprint along the west basin margin, which is also marked by outcrops of unit **rtu**. The local geohistory that emerges includes (1) formation of **rtu**; (2) basin formation accompanied by the development of a concentric fracture/fault zone; (3) pancake dome formation, with local reactivation of concentric fractures; and (4) shield terrain evolution, including formation of north-striking fractures and generally east-trending wrinkle ridges, all developing in a time-transgressive fashion, broadly overlapping in time and space. Unit **rtu** is notably free of concentric fractures or any evidence that it was affected by the development of Allatu. Like Dhisana, Allatu shows a notable lack of radial fractures, obvious flows, and any evidence of early dome formation.

Bhumiya Corona

Bhumiya Corona (150 km diameter; lat 15° N., long 118° E), an approximately 600 m deep circular basin nestled among exposures of unit **rtu**, displays a circular 75–100-km-wide fracture/fault zone. The fracture zone, best preserved along the north-northeastern, southwestern, and western margins is variably masked by unit **S**. Unit **S** occurs in a lace-like continuous fashion from the surrounding lowlands, across the basin walls and into the basin interior. Bhumiya lacks an interior peak or high, but two pancake domes occur to the northwest of Bhumiya, barely overlapping the location of the concentric fracture zone. Wrinkle ridges trend eastward across the structure, parallel to regional trends, and deform shield terrain material. The local geohistory that emerges includes (1) formation of **rtu** and **rtHG**; (2) basin formation accompanied by the development of a concentric fracture/fault zone; (3) pancake dome formation;

and (4) shield terrain evolution, including formation of north-striking fractures and generally east trending wrinkle ridges, all developing in a time-transgressive fashion, broadly overlapping in time and space. Bhumiya lacks radial fractures, obvious flows, and any evidence that an earlier domical structure existed during its evolution.

Omeciuatl Corona

Omeciuatl Corona (125 x 175 km diameter; lat 16.5° N., long 118.5° E.), located just north of Bhumiya, includes an elongate 600–700-m-deep basin. The deeper depth of these two circular lows is likely a function of their location nestled among ribbon-tessera terrain and, hence, higher elevation surroundings. Omeciuatl's 30–100-km-wide concentric fracture/fault zone conforms to the shape of the elongated basin with fractures developed on the basin walls and cutting the adjacent region, including locally cutting nearby tessera terrain. Wrinkle ridges, parallel to regional trends, deform unit **S** across the lowland, within and across Omeciuatl basin walls and floor, and between individual exposures of unit **rtu**. The local geohistory that emerges includes (1) formation of **rtu** and **rtHG**; (2) basin formation accompanied by the development of concentric fracture/fault zone; and (3) shield terrain evolution, including formation of north-striking fractures and generally east-trending wrinkle ridges, all developing in a time-transgressive fashion, broadly overlapping in time and space. Omeciuatl lacks radial fractures, obvious large flows, and any evidence of early uplift or doming history.

The concentric fracture zones of Omeciuatl and Bhumiya just barely touch one another, but relative temporal relations between the two are indistinguishable—both circular low structures postdate formation of tessera terrain tectonic fabrics and predate the formation of northerly striking fractures, shield terrain development, and wrinkle ridge formation. Allatu shows similar relative temporal relations within its local environment. Dhisana lies too far from **rtu** inliers (~150 km) to be able to place robust temporal constraints on Dhisana tessera-terrain formation, but the preserved relations are certainly consistent with temporal relations delineated for the other circular lows.

Rosmerta Corona

Rosmerta Corona (~300 km diameter; centered at lat 0° N., long 124.5° E. in V-24 and V-36) is more typical of a radial concentric corona (Stofan and others, 1992) marked by well-developed radial fractures (which do not extend into the map area) and flows. Although the center of Rosmerta lies outside the map area, Rosmerta flows flood local lows across southeastern Haastse-baad Tessera within the map area. Radial fractures clearly crosscut ribbon-tessera fabric in V-24, providing clear evidence that Rosmerta Corona formed after the development of the distinctive tessera-terrain fabric. Rosmerta flows also fill local structural basins within unit **rtHG**, indicating that intra-tessera basin formation predated Rosmerta formation. Rosmerta flows are generally radar smooth with local shields.

Formation of circular lows

The five circular lows share many characteristics, yet they differ from typical radial concentric coronae. The circular lows are marked by (1) circular basins that lie 300–900 m below local base level, with (2) apparent spatial association with tessera terrain, and (3) well-developed concentric fracture/fault zones that correlate spatially with basin wall topography but also extend into the adjacent lowlands. The structures show a notable lack of radial fractures, long flows, and evidence for early doming or uplift. In contrast, radial concentric coronae, as represented by Rosmerta Corona, are marked by positive topography, radial fracture suites, and variably developed volcanic flows (Stofan and others, 1992, 1997, 2001). Radial concentric coronae are also commonly clustered in spatial association with volcanic rises, occur as chains associated with chasmata, and occur between volcanic rises (Stofan and others, 1992, 2001; Hamilton and Stofan, 1996; DeLaughter and Jurdy, 1999), whereas circular lows may reside more typically within the lowlands (Shankar and Hansen, 2008). Although many workers accept that (all) coronae represent the surface expression of endogenic diapirs that impinged on the crust or lithosphere (Janes and others, 1992; Squyres and others, 1992; Stofan and others, 1992, 1997; Janes and Squyres, 1995; Koch and Manga, 1996; Smrekar and Stofan, 1997; DeLaughter and Jurdy, 1999), geologic relations preserved at the circular lows within the map area may be difficult to justify within a diapiric hypothesis. Efforts aimed at modeling the surface expression of diapir emplacement consistently predict early surface doming and development of radial fractures that extend beyond the limits of the subsurface diapir (Withjack and Scheiner, 1982; Cyr and Melosh, 1993; Koch and Manga, 1996; Smrekar and Stofan, 1997). Could circular lows represent diapiric structures, yet lack radial fractures? Perhaps radial fractures formed, but were buried by later flows (for example, the volcanic loading model of Cyr and Melosh (1993)). Such an explanation would not address the lack of radial fractures in adjacent exposed tessera terrain, which should preserve a record of radial fractures (if they had formed), nor does it address the fact that circular lows form topographic basins, not domes. The lack of radial fractures might be attributed to regional stress fields that accompanied diapir emplacement (Withjack and Scheiner, 1982), but this would result in formation of an elliptical central domain, which should display positive rather than negative topography. Although Dhisana and Omeciuatl describe somewhat elongate basins, there is no evidence that regional deviatoric stresses of the required orientation (east-west-oriented maximum compressive stress; north-south-oriented minimum compressive stress) existed during basin evolution. The long axis of both Dhisana and Omeciuatl are incompatible with possible fabric weakness imposed by tessera-terrain fabrics, and north-striking extension fractures might record principle stress orientations 90° from the principle stress orientations predicted by basin shape. Perhaps the rheological character of the local crust was such that radial fractures never formed, or the host ribbon terrain somehow limited radial fracture formation. Rosmerta Corona seems to challenge these explanations, because radial fractures associated with Rosmerta extensively

dissect and crosscut ribbon-terrain fabric of Haastse-baad Tessera (Bleamaster and Hansen, 2005). Therefore, it would seem that (1) there is something unique about the rheological conditions associated with the formation of circular lows as diapirs, (2) circular lows formed by a different mechanism than radial-domical coronae, or (3) both.

Perhaps these circular lows do not represent the surface expression of subsurface diapirs. Other hypotheses have been proposed for corona evolution, including formation as volcanic caldera, as sinkholes due to subsurface flow or negative diapirs, and by exogenic impactors (Shankar and Hansen, 2008; Hansen and others, 2008). If circular lows represent caldera, we might expect extensive associated flows, as well as collapse features within the interior basins walls (Lipman, 2000); but, such features are not observed. In addition, the concentric fracture zones associated with each circular low extend well outside the circular basins into the surrounding lowland, which would not be expected in the case of magma chamber collapse.

Circular lows could represent impact craters that differ from their pristine cousins. Vita-Finzi and others (2005) suggested that almost all coronae represent impact craters, and Hamilton (2005) proposed that all coronae, as well as all circular features on Venus, represent impact craters. These geologists suggest that coronae may represent impact craters modified by erosion. If circular lows were modified by erosion, we might expect to see drainage patterns indicative of erosive processes showing material transport both toward the basin interior and outward from it; such features are not observed. In addition, the variable blanketing of the concentric fracture zones by shields would not seem to be easily accommodated in such a scenario.

Circular lows within the map area could differ from pristine impact craters due to differences in host rheology during initial formation, rather than as a result of postformational modifications; or they could represent subsurface processes, either negative diapirs or subsurface flow. Each of the circular lows lies nestled among inliers of ribbon terrain, and these features could have formed during the evolution of ribbon terrain. This hypothesis might address (1) the basin morphology; (2) the concentric fracture zone relative to basin topography; (3) relative timing and spatial association with ribbon terrain; (4) the cookie-cutter form of circular lows relative to adjacent ribbon terrain; and (5) the lack of obvious lava flows, radial fractures, and evidence of an early uplift history.

Dorsa

Unelanuhi Dorsa, a 150–250-km-wide and over 1,000-km-long ridge belt within the map area, extends westward for ~1,000 km into V–22. Unelanuhi Dorsa comprises a northwest-trending linear rise, ~500 m high, that preserves an internal fabric marked by closely spaced folds and fractures. Internal fold fabrics trend parallel to Unelanuhi Dorsa, as well as at a slightly oblique angle; fractures strike more northerly. The oblique fractures could have formed prior to dorsa formation or synchronous with dorsa uplift. Early-formed fractures would have been uplifted and protected from burial within the adjacent lowlands. Unelanuhi Dorsa trends northwest, parallel to the northeast boundary of Ovda Regio. It is possible that the fold

ridges of this dorsa, and perhaps the dorsa itself, are genetically related to Onda crustal plateau formation; however, given the paucity of data such an interpretation is speculative.

Geologic History

A relatively simple geologic history of the map area emerges. Basal terrain units formed across the map area in a time-transgressive manner, followed by local formation of circular low features. Extensively developed shield terrain evolved time-transgressively across the region coupled with formation and reactivation of regional fractures, formation of wrinkle ridges, and the development of inversion structures. Rosmerta Corona flows, smooth flows undivided, and flows from the northwest volcano flooded local topographic lows. Impact craters, scattered across the surface, likely formed only after local ribbon-tessera-terrain material gained strength enough to act in a brittle fashion with regard to bolide impact. Circular lows may represent exogenic bolide impact or endogenic subsurface processes that formed prior to complete strengthening of local ribbon-tessera terrain.

Basal terrain units *rtO*, *rtHG*, *rtu*, and *frN* occur within the same stratigraphically constrained position across the map area, and temporal relations among the various basal terrains cannot be robustly differentiated. This means that there is no evidence to suggest that these terrains form synchronously, nor is there evidence that requires that the various basal terrains formed in a time-transgressive fashion across the map area. Based on the similar orientation in structural fabric of *rtHG* and *rtu*, the simplest interpretation is that this tessera terrain fabric may have formed as a coherent unit across much of the map area, particularly in the eastern region. Unit *rtO* defines a distinctly different fabric orientation than units *rtHG* and *rtu*, and as such, it likely records a spatially separate and likely temporally distinct event. Unit *rtO* also resides at distinctly higher elevations than units *rtHG* and *rtu*, which is consistent with the interpretation of a separate evolution of *rtO*. Basal terrain *frN* dominates kipukas preserved across the northwestern part of the map area. Although unit *frN* might exist under much of the northwestern map area, it is likely that unit *frN* represents a composite unit, variably developed in both space and time. In many small exposures, unit *frN* may represent unit *rtu* veiled by a thin veneer, locally reactivated along *rtu* structures. Intratessera basin units (units *itbO* and *itbHG*) formed after the development of their associated tessera terrain fabric but before adjacent shield terrain, although it is possible that shield terrain began to form concurrently with units *itbO* and *itbHG*.

The mode of formation of ribbon-tessera terrain is outside the scope of the current discussion. Ribbon-tessera fabrics have been variably interpreted as the result of significant crustal shortening associated with the interaction of a mantle downwelling on thin lithosphere (Bindschadler and Parmentier, 1990; Bindschadler and others, 1992a,b; Bindschadler, 1995), the interactions of a large thermal mantle plume with thin lithosphere (Hansen and others, 1997; Phillips and Hansen, 1998; Hansen and Willis, 1998; Ghent and Hansen, 1999; Hansen and others, 1999, 2000), and progressive solidification and deforma-

tion of the surface of huge lava ponds resulting from massive partial melting of the mantle as a result of large bolide impact with ancient thin lithosphere (Hansen, 2006). The presence of a wide range of extensional and contractional wavelengths from Magellan SAR effective resolution to tens of kilometers, and synchronous flooding of local topographic lows by low viscosity fluid (lava) favors the lava pond hypothesis (Hansen, 2006). The downwelling and plume crustal plateau hypotheses call for plateau formation associated with crustal thickening, the former by crustal shortening and the later by magmatic accretion. In both hypotheses it is postulated that crustal plateaus sit high due to thickened crust; lowland ribbon-tessera terrain, such as that preserved across the map area, would require collapse of the plateau crust with time, which may be difficult to accommodate based on modeling (Nunes and others, 2004). In the case of plateau formation via crystallization of a bolide-impact-induced lava pond, low density mantle that results from massive partial melting supports the plateau; and it is possible that the low density mantle root could be removed through later mantle circulation processes resulting in plateau subsidence to a lowland position (Hansen, 2006). At this point it is premature to dismiss any hypotheses of crustal plateau and ribbon terrain formation. Perhaps future studies of ribbon terrain at a global scale will lead to hybrid hypotheses that accommodate the relations preserved within the map area.

Shield terrain consistently lies stratigraphically above the basal terrains at each individual location; thus, shield terrain at any one location postdates the formation of basal-terrain units at that same location. However, given the lack of robust temporal relations (relative or absolute) between the various basal terrain units, we cannot robustly state (or deny) that all shield terrain postdates the formation of all ribbon-tessera terrain. In addition, map relations indicate that unit *S* developed time-transgressively at both the local and regional scale.

The five circular lows formed after the formation of their local tessera terrain fabric but before dominant formation of shield terrain and the development of north-striking fractures at each particular location. It is possible that local shield terrain began to evolve early, but in any case, local shield terrain formation continued after the formation of each circular low. Northerly striking fracture suites postdated formation of each local circular low. Fractures were locally reactivated during the evolution of shield terrain. Wrinkle-ridge formation overlaps temporally with the development of shield terrain. The temporal location of circular lows forming after local ribbon terrain fabric, but before complete development of shield terrain, is consistent with circular-low formation via bolide impact on an ancient, partially crystalline lava-pond surface.

The eruption of the northwest volcanic material and the formation of Rosmerta Corona—marked by domical uplift, radial fracture formation, and the emergence of radially distributed lava flows—are unconstrained with regard to one another. Both events formed relatively recently in recorded local history, possibly overlapping in time with the formation of local shield terrain. The pristine impact craters within the map area postdate local formation of tessera-terrain tectonic fabric, emplacement of units *itbO* and *itbHG*, and the formation of circular lows. The relative timing of local shield terrain and individual impact cra-

ters is difficult to robustly constrain given that individual shields could form before and after impact craters. Impact craters that have radar-smooth interiors and lack haloes are relatively older than impact craters that have haloes and radar-rough interiors (Izenberg and others, 1994; Phillips and Izenberg, 1995).

Implications for Venus Lowland Resurfacing Processes

Several hypotheses have emerged to address the near random distribution of ~970 apparently pristine impact craters across the surface of Venus (Schaber and others, 1992; Phillips and others, 1992; Herrick and others, 1997; Basilevsky and others, 1997). Because impact-crater density reflects the relative age of planet surfaces, the near random spatial distribution of craters indicates that Venus lacks large regions of very young and very old surfaces. The paucity of small craters, due to screening by Venus' thick atmosphere, hampers surface age determination. In addition, determination of surface age by crater density requires binning across a range of crater diameters—a technique not possible on Venus. A datable surface on Venus must exceed $\sim 2 \times 10^7$ km² in order to be statistically robust, based on impact crater density alone (Phillips and others, 1992), and areas this large require assumptions with regard to surface formation that severely limit the uniqueness of any temporal or history interpretation (Campbell, 1999). Although some workers combine morphologically similar units into large composite regions for crater-density dating (Namiki and Solomon, 1994; Price and Suppe, 1994; Price and others, 1996; Basilevsky and Head, 2002), these studies assume all terrains formed at the same time, and lack statistical validity (Campbell, 1999).

Resurfacing hypotheses are broadly divisible into two groups: (1) catastrophic/episodic and (2) equilibrium/evolutionary (Hansen and Young, 2007). Catastrophic/episodic hypotheses propose that a global-scale, temporally punctuated event or events dominated Venus' evolution, which is reflected in the generally uniform impact crater distribution (Schaber and others, 1992; Strom and others, 1994; Herrick, 1994). Equilibrium/evolutionary hypotheses suggest, instead, that the generally uniform crater distribution results from relatively continuous resurfacing in which volcanism and (or) tectonism occur across the planet through time, although the style of resurfacing could vary spatially and temporally at any given locale (Phillips and others, 1992; Guest and Stofan, 1999). Equilibrium/evolutionary hypotheses could also involve a progression from global, steady-state equilibrium resurfacing to global impact crater accumulation as a result of secular changes (Solomon, 1993; Phillips and Hansen, 1998; Bjonnes and others, 2008).

Catastrophic hypotheses include (1) a one-dimensional lithospheric instability hypothesis which calls for wholesale lithospheric recycling (Parmentier and Hess, 1992; Turcotte, 1993; Turcotte and others, 1999) and (2) volcanic burial of a preserved lithosphere (Schaber and others, 1992; Steinbach and Yuen, 1992; Strom and others, 1994). Because these hypotheses assume global synchronicity, they predict a single average model

surface age (AMSA), marking the time of the last lithospheric catastrophe. However, Phillips and Izenberg (1995) document three AMSA provinces based on impact crater density and crater morphology that is inconsistent with catastrophic resurfacing.

Near-global catastrophic flooding is incorporated into the global stratigraphy hypothesis (Basilevsky and Head, 1995, 1998; Head and Basilevsky, 1998), which predicts global eras represented by different geologic processes: (1) early, globally extensive and synchronous tessera-terrain deformation (and resulting impact crater destruction), (2) local warping and crustal thickening, forming isolated high-standing crustal plateaus and the extensive lowlands; and (3) catastrophic emplacement of 1–3-km-thick flood lava burying earlier formed impact craters across the lowlands. Wrinkle ridges deform lowland flood lavas, whereas the highland regions marked by crustal plateaus preserve remnant tessera terrain, preserving the only record of precatastrophic flooding processes.

Evolutionary resurfacing hypotheses, which call for equilibrium or steady-state resurfacing, may include different modes of impact crater accumulation through time. Phillips (1993) proposed an equilibrium volcanic resurfacing hypothesis, which calls for near steady-state impact-crater formation and burial (destruction) through spatially random volcanic activity across local areas ($\sim 10^7$ km², or less). The resulting equilibrium resurfacing represents a balance between crater formation and burial integrated across space and time. Although the equilibrium volcanic resurfacing hypothesis is dominantly statistical, it specifies that craters were removed by volcanic burial; therefore, it can be tested by geologic observations. The equilibrium volcanic resurfacing hypothesis does not specifically address tessera-terrain formation or any relation between impact craters and tessera terrain. Guest and Stofan (1999) propose a nondirectional equilibrium surface evolution in which coronae, rifts, wrinkle ridges, small and large edifices, and large flow fields formed throughout the portion of Venus' history revealed by presently exposed rock units. They suggest that the lowlands accumulated lavas erupted in a range of spatially and temporally transgressive styles. Their hypothesis does not address the formation of tessera-terrain units. However, the nondirectional evolution hypothesis seems to call for volcanic burial of ancient impact craters.

Each hypothesis calls for emplacement of thick lava flows (~ 1 km), whether emplaced catastrophically or partitioned over time, across large expanses of the lowlands in order to bury pre-existing impact craters. We can test the requirement of such a thick (1 km) layer across much of the map area. Unit *rtu* occurs in small exposures across much of the map area. In many cases unit *rtu* is exposed in regions of locally higher (although still quite gentle) topographic slopes. The outcrop of unit *rtu* north of Barrera Crater (lat 18.5° N., long 109.5° E.) has an average slope of $\sim 0.286^\circ$ and shows a break in slope just outside the shield-rich region. Rounding this slope to 0.3° , we determine a 1-km isopach surface, indicating where ribbon-tessera terrain could lie beneath a 1-km-thick cover and, therefore, harbor buried impact craters. The majority of the map area cannot accommodate a 1-km-thick layer stratigraphically above ribbon-tessera terrain.

A similar isopach constructed for unit frN is also shown on the geologic map. The slopes associated with exposures of unit frN are generally less than the slopes associated with unit rtu, therefore maximizing the region that could hide buried impact craters. Despite the conservative approach of this exercise, taken together, the two isopach contours indicate that essentially no part of the map area could accommodate a layer >1 km thick stratigraphically above ribbon-tessera terrain or the fracture terrain units. Yet both of these units are predicted to predate the emplacement of the 1–3 km thick regional plains required within the context of the catastrophic resurfacing and global stratigraphy hypotheses. Neither the volcanic equilibrium resurfacing hypothesis nor the nondirectional hypothesis directly imply that a thick layer lies above tessera terrain, yet both hypotheses call for thick lava packages to bury early formed impact craters. Each of these hypotheses require large areas of the Venusian surface to have thick regional plains, but the overall shape of the regional plains at such depths is important. The occurrence of exposures of basal units, those inferred to predate regional plains (units rtu, rtHG, rtO, frN) across the map area, indicates that first-order geologic map relations within the map area are inconsistent with the predictions or requirements of the catastrophic resurfacing, global stratigraphy, volcanic equilibrium resurfacing, and nondirectional resurfacing hypotheses.

Similar first-order map relations exist across the map area, in V–24 to the east and in V–11 and V–12 to the north (Aubele, 1996). Across each of these four adjacent quadrangles, a thin veneer of shield terrain lies directly above ribbon-tessera terrain and (or) fracture terrain, presenting a major challenge to all resurfacing hypotheses that call for burial of impact craters. In fact, these first-order map relations provide strong evidence that impact craters could not have formed on surfaces marked by ribbon-tessera terrain and fracture terrain and have been subsequently buried.

Solomon (1993) proposed a hybrid two-stage surface history for Venus that did not require burial of impact craters. Solomon (1993) called for viscous relaxation of ancient impact craters, followed by later crater accumulation. According to his hypothesis, early steady-state impact-crater formation and destruction resulted from global-scale tectonic deformation (viscous relaxation of impact craters) driven by extremely high heat flow; cooling led to a change in crustal rheology and subsequent accumulation of impact craters across the surface. In this hypothesis, Venus' surface could not preserve impact craters until it cooled significantly; once cooled, the surface accumulated craters since the time of the global rheological transition, interpreted as the global AMSA. This hypothesis does not require the emplacement of thick regional plains, because it does not require impact crater burial. It does, however, require that the surface of Venus was rheologically weak at the global scale. Subsequent to the proposal of this hypothesis, new flow laws determined for ultra-dry diabase (Mackwell and others, 1998) indicated that Venus' crust is too strong, even at elevated surface temperature, to allow for early viscous relaxation of impact craters as hypothesized. Although Solomon's (1993) hypothesis seems to have been abandoned in light of the new flow laws, the spirit of the hypothesis might be

feasible if ancient Venus was wetter than contemporary Venus, resulting in possible regional or local viscous flow, perhaps enhanced by local thermal anomalies. Given that Solomon's hypothesis does not require a thick lava package to bury impact craters, this hypothesis remains viable based on map area relations.

The spirit of Solomon's (1993) hypothesis might also be preserved in a modified hypothesis in which craters could be destroyed (rather than buried) at local spatial scale and in a time-transgressive fashion. Hansen and Young (2007) proposed such a two-stage resurfacing hypothesis. That hypothesis, herein called the SPatially Isolated Time-Transgressive Equilibrium Resurfacing (SPITTER) hypothesis, calls for early equilibrium resurfacing, with a later transition to crater accumulation. In contrast to Solomon, who calls for global formation of tessera terrain, these workers call on spatially isolated, time-transgressive destruction of ancient impact craters through local formation of ribbon terrain. Coherent tracts of tessera terrain could have evolved in a spatially isolated but time-transgressive fashion (Bindschadler, 1995; Hansen and Willis, 1996, 1998) and as allowed by the relations across the map area (and V–24). The SPITTER hypothesis does not depend on a particular mechanism of ribbon-tessera formation (such as downwelling, plume, or impact-induced lava pond), but rather focuses on the similarities of each of these hypotheses: complete crater destruction in a spatially isolated yet time-transgressive fashion.

According to the SPITTER hypothesis, crustal plateau formation and subsequent collapse to form lowland tessera terrain, coupled with a transition from thin to thick lithosphere, might accommodate the various observations and correlations across Venus. Observations related to impact craters include the following:

1. Venus shows few partially flooded and few faulted craters (Herrick and others, 1997); most craters appear pristine. Although studies indicate some modification (Sharpton, 1994; Wichman, 1999; Herrick and Sharpton, 2000), examples of near complete flooding of craters are rare. Thus, crater destruction was an all or nothing endeavor. Craters are not preserved, form but viscously relax, are completely destroyed by tectonism, are buried beyond recognition, or are preserved in a near-pristine state.
2. Large craters (>100 km diameter) have rim-terrain heights of ~650 m (Herrick and Sharpton, 2000); thus, burial requires strata >650 m. Presumably ancient craters would far exceed Venus' largest crater and likely require ~1-km-thick strata for burial.
3. Mapping across V–23 and V–24 indicates that large tracts of lowland tessera show thin blanketing of strata (this study). Additionally, huge lowland regions (>10⁶ km²) are covered by thin layers or flows tens of meters to 100 m thick (Guest and others, 1992; Aubele, 1996; DeShon and others, 2000; Addington, 2001; Hansen and DeShon, 2002; Stofan and others, 2005).
4. Craters on ribbon-tessera terrain postdate tessera fabric formation (Gilmore and others, 1997).
5. Craters record a temporal sequence of degradation in which halos are lost and troughs and interiors fill with smooth material over time (Izenberg and others, 1994;

Herrick and Sharpton, 2000); thus, craters are divisible into broad relative age groups. Young craters display haloes and rough interiors. Old craters lack haloes and have smooth interiors. Intermediate craters lack haloes and display rough interiors.

6. Crater density combined with crater morphology (5) allows delineation of three AMSA provinces (Phillips and Izenberg, 1995). Spatial correlation of geologic time-dependent criteria (halos) with crater density suggests that AMSA provinces reflect true temporal domains, not stochastic fluctuations in a random distribution (Campbell, 1999).
- In addition, comparison of AMSA provinces with major geologic (Hansen and Young, 2007) features reveals several observations:
7. Volcanic rises show no correlation with AMSA.
8. Crustal plateaus correlate mostly with intermediate AMSA.
9. Many lowlands correlate with old AMSA.
10. Beta-Atla-Themis and Lada, regions of volcanotectonic activity (Crumpler and others, 1997), correlate with young AMSA.

SPITTER (fig. 12) accommodates observations 1–10 above. The global AMSA might record, broadly, the time of a change from near steady-state crater formation and destruction (thin lithosphere) to crater accumulation (thick lithosphere), whereas the distinct AMSA provinces occur as outlined above. The SPITTER hypothesis accounts for complete local crater destruction and for pristine craters (1, 2), yet it accommodates the occurrence of thin, rather than thick, lava flows (3). It predicts that craters should not record tessera deformation (4), and it allows for the preservation of stages of crater degradation (5) and the occurrence of distinct AMSA provinces (6), with specific geologic relations (7–10).

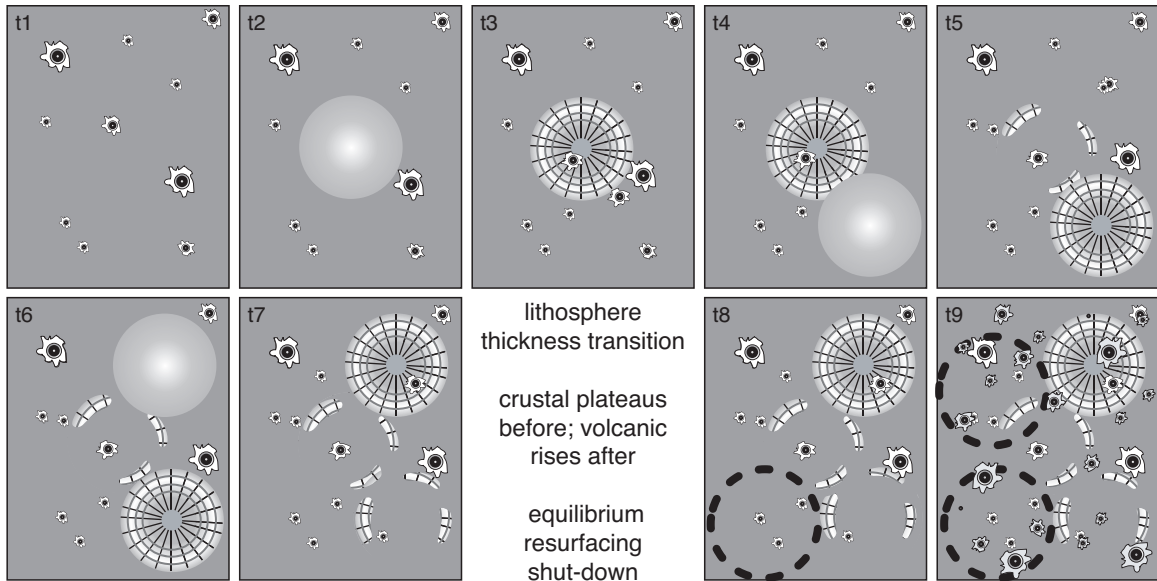
The SPITTER hypothesis embodies the spirit of the equilibrium volcanic hypothesis (Phillips, 1993), accommodates broad aspects of the view that volcanotectonic processes occurred across Venus through time, though styles and locations have changed (Guest and Stofan, 1999), and incorporates a secular change in resurfacing and dynamic processes (Solomon, 1993; Grimm, 1994; Solomatov and Moresi, 1996; Schubert and others, 1997; Phillips and Hansen, 1998), which could address some aspects of a broadly defined geologic history that might accommodate some eras highlighted by the global stratigraphy hypothesis (Basilevsky and Head, 1995, 1998, 2002).

Summary

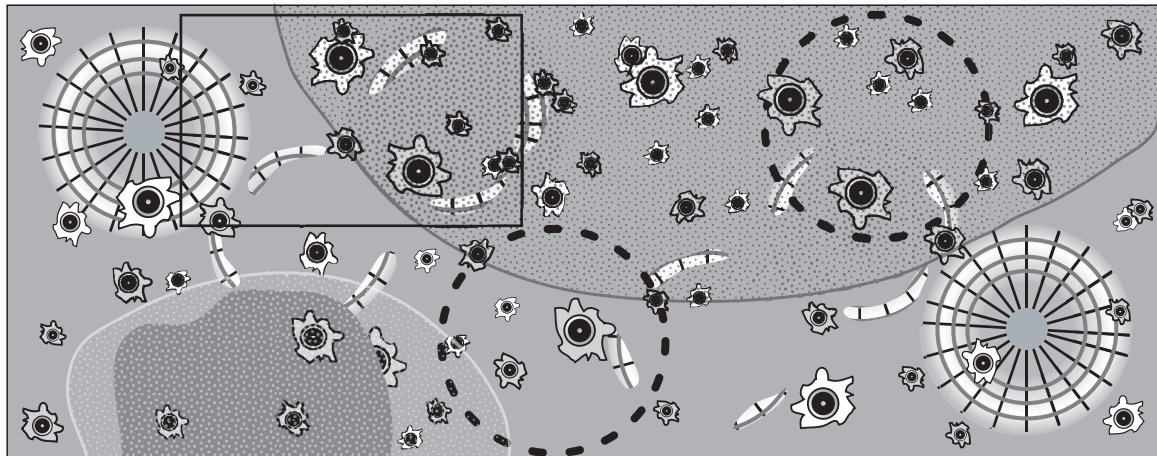
In summary, shield terrain comprises the most prominent unit across the map area. Shield terrain forms a thin lace-like veneer of shields and low viscosity shield paint; it occurs across a range of elevations; it postdates and lies directly upon ribbon terrain in the eastern part of the map area and on fracture terrain in the western part of the map area. In both cases, shield terrain locally covers or veils the units that serve as its basement. Shield terrain apparently formed by local point-source eruption across the map area. Shield paint coalesced into a mechanically coherent layer that was able to fracture and to deform into wrinkle ridges and polygonal fabrics.

The interactions among fractures, wrinkle ridges, and shield-terrain emplacement imply diachronous wrinkle ridge evolution, fracture reactivation, and shield-terrain evolution. Locally north-trending ridges represent inversion structures formed as a result of the filling of north-striking fractures with shield-terrain material and subsequent regional contraction and structural inversion of the fill into north-trending ridges. The interaction of shield terrain, wrinkle ridges, and fractures also indicates that shield terrain material forms a thin veneer, rather than a thick layer.

Ribbon-tessera terrain is divisible into two or three distinct packages based on fabric orientation and elevation. Ribbon-tessera terrain of Ovda Regio likely formed temporally separate from ribbon terrain of Haastse-baad-Gegute Tesserae, which formed distinct from Thetis Regio ribbon-tessera terrain to the south in V–36. Undivided ribbon-tessera terrain displays patterns in its tectonic fabric that might indicate a genetic relation with Haastse-baad-Gegute Tesserae. Circular lows, a distinctive class of coronae features marked by circular basins and concentric fractures zones, differ from many coronae, notably lacking radial fractures, long lava flows, and positive topography. Circular lows might represent a different class and perhaps a different origin from other coronae. Circular lows may represent impact craters formed late during the evolution of local ribbon-tessera terrain. Such a proposal will require testing by additional geologic mapping across the planet. Geologic relations across the map area do not support the occurrence of equilibrium volcanic resurfacing, catastrophic global resurfacing, or near-global (global stratigraphy) resurfacing, all of which require burial of ancient impact craters.



A



B



Figure 12. Illustration showing proposed evolution of Venusian surface. **A.** Time-step cartoons (t1–t9) illustrating the evolution of the SPIT-TER hypothesis for Venus resurfacing. t1, Initially the surface accumulates impact craters. t2, As a crustal plateau forms on thin lithosphere, impact craters within the plateau aureole are destroyed; t3, characteristic ribbon-terrain fabrics mark the plateau, which can accumulate new impact craters. t4, A new, spatially separate plateau forms on thin lithosphere, erasing impact craters within its aureole. t5, As the second plateau evolves and becomes able to preserve newly formed impact craters, the first formed plateau could topographically decay. But ribbon-terraza fabrics survive, except where buried by local thin volcanic material; impact craters are not buried. t6–t7, As new plateaus form on the thin lithosphere, impact craters are removed locally and earlier formed plateaus are variably covered with thin flows. t8, These processes continue until a secular change results in globally thick lithosphere. Crustal plateaus that formed just prior to the secular change stand high. Crustal plateaus cannot form on thick lithosphere by any of the three hypothesized mechanisms; however, volcanic rises could form above a large thermal mantle diapir (dashed circle). During volcanic rise formation, impact craters are not erased, because the lithosphere is too thick for crater destruction via subsurface processes. Volcanic rise formation raises the local altitude of the surface but does not affect impact crater density, except by local volcanotectonic processes. The entire global surface becomes one of impact crater accumulation (t8, t9), except local areas of concentrated volcanotectonic activity where impact craters are buried by surface lava flows, such as the Beta-Alta-Themis and Lada regions (outside of map area). **B.** A composite cartoon surface schematically illustrating three average model surfacing age (AMSA) provinces that would emerge from surface evolution described in A. Old AMSA provinces would include lowland regions where ancient crustal plateaus formed (tessera-terrain inliers) or no crustal plateaus form (black stipple). Young AMSA provinces would include areas affected by recent volcanotectonic activity (dark gray shaded area) that buried both impact craters and their halos (white stipple), such as Beta-Alta-Themis and Lada regions. Intermediate AMSA provinces would include high-standing crustal plateaus and lowland regions with tessera-terrain inliers marking ancient crustal plateaus. Boundaries between AMSA provinces would not be sharp as illustrated. Note that volcanic rises could correlate with any of the AMSA provinces, because volcanic rise formation would only affect the local AMSA if rise formation included extensive volcanotectonic burial of impact craters. In general, rise formation simply elevates a pre-existing surface but does not otherwise affect impact crater density or morphology. Rectangle outlines area conceptually similar to the surface history of the map area. Figure modified from Hansen and Young (2007).

References Cited

- Addington, E.A., 2001, A stratigraphic study of small volcano clusters on Venus: *Icarus*, v. 149, p. 16–36.
- Anderson, F.S., and Smrekar, S.E., 1999, Tectonic effects of climate change on Venus: *Journal of Geophysical Research*, v. 104, p. 30,743–30,756.
- Arvidson, R.E., Greeley, R., Malin, M.C., and 5 others, 1992, Surface modification of Venus as inferred from Magellan observation of plains: *Journal of Geophysical Research*, v. 97, p. 13,303–13,318.
- Aubele, J., 1996, Akkruva small shield plains—Definition of a significant regional plains unit on Venus [abs.]: *Lunar and Planetary Science*, v. XXVII, p. 49–50.
- Baker, V.R., Komatsu, G., Gulick, V.C., and Parker, T.J., 1997, Channels and valleys, in Bouger, S.W., Hunten, D.M., and Phillips, R.J., eds., *Venus II: Tuscon*, University of Arizona Press, p. 757–798.
- Baker, V.R., Komatsu, G., Parker, T.J., and 3 others, 1992, Channels and valleys on Venus—Preliminary analysis of Magellan data: *Journal of Geophysical Research*, v. 97, p. 13,395–13,420.
- Banerdt, W.B., McGill, G.E., and Zuber, M.T., 1997, Plains tectonics on Venus, in Bouger, S.W., Hunten, D.M., and Phillips, R.J., eds., *Venus II: Tuscon*, University of Arizona Press, p. 901–930.
- Banerdt, W.B., and Sammis, C.G., 1992, Small-scale fracture patterns on the volcanic plains of Venus: *Journal of Geophysical Research*, v. 97, p. 16,149–16,166.
- Banks, B.K., and Hansen, V.L., 2000, Relative timing of crustal plateau magmatism and tectonism at Tellus Regio, Venus: *Journal of Geophysical Research*, v. 105, p. 17,655–17,668.
- Basilevsky, A.T., and Head, J.W., 1995, Global stratigraphy of Venus—Analysis of a random sample of thirty-six test areas: *Earth, Moon, and Planets*, v. 66, p. 285–336.
- Basilevsky, A.T., and Head, J.W., 1998, The geologic history of Venus—A stratigraphic view: *Journal of Geophysical Research*, v. 103, no. E4, p. 8531–8544.
- Basilevsky, A.T., and Head, J.W., 2002, Venus—Timing and rates of geological activity: *Geology*, v. 30, no. 11, p. 1015–1018.
- Basilevsky, A.T., Head, J.W., Schaber, G.G., and Strom, R.G., 1997, The resurfacing history of Venus, in Bouger, S.W., Hunten, D.M., and Phillips, R.J., eds., *Venus II: Tucson*, University of Arizona Press, p. 1047–1086.
- Bilotti, F., and Suppe, J., 1999, The global distribution of wrinkle ridges on Venus: *Icarus*, v. 139, no. 1, p. 137–157.
- Bindschadler, D.L., 1995, Magellan—A new view of Venus geology and geophysics: *Reviews in Geophysics*, v. 33, p. 459–467.
- Bindschadler, D.L., deCharon, A., Beratan, K.K., and Head, J.W., 1992a, Magellan observations of Alpha Regio—Implications for formation of complex ridged terrains on Venus: *Journal of Geophysical Research*, v. 97, p. 13,563–13,577.
- Bindschadler, D.L., Schubert, G., and Kaula, W.M., 1992b, Coldspots and hotspots—Global tectonics and mantle dynamic of Venus: *Journal of Geophysical Research*, v. 97, p. 13,495–13,532.
- Bindschadler, D.L., and Head, J.W., 1991, Tessera terrain, Venus—Characterization and models for origin and evolution: *Journal of Geophysical Research*, v. 96, p. 5889–5907.
- Bindschadler, D.L., and Parmentier, E.M., 1990, Mantle flow tectonics—The influence of a ductile lower crust and implications for the formation of topographic uplands on Venus: *Journal of Geophysical Research*, v. 95, no. B13, p. 21,329–21,344.
- Bjonnes, E.E., Hansen, V.L., and Swenson, J.B., 2008, Results of equalibrium resurfacing Monte Carlo models on Venus [abs.]: *Lunar and Planetary Science*, v. XXXIX, abstract 2410 [PDF].
- Bleamaster, L.F., III, and Hansen, V.L., 2005, Geologic map of the Ovda Regio quadrangle (V–35), Venus: U.S. Geological Survey Geologic Investigations Series I–2808, scale 1:5,000,000 [<http://pubs.usgs.gov/imap/i2808/>].
- Brown, C.D., and Grimm, R.E., 1999, Recent tectonic and lithospheric thermal evolution of Venus: *Icarus*, v. 139, no. 1, p. 40–48.
- Buchanan, J.G., and Buchanan, P.G., eds., 1995, Basin inversion: *Geological Society of London Special Publication* 88, 596 p.
- Campbell, B.A., 1999, Surface formation rates and impact crater densities on Venus: *Journal of Geophysical Research*, v. 104, no. E9, p. 21,951–21,955.
- Chapman, M.G., and Zimbelman, J.R., 1998, Corona associations and their implications for Venus: *Icarus*, v. 132, no. 2, p. 344–361.
- Crumpler, L.S., Aubele, J.C., Senske, D.A., and 3 others, 1997, Volcanoes and centers of volcanism on Venus, in Bouger, S.W., Hunten, D.M., and Phillips, R.J., eds., *Venus II: Tucson*, University of Arizona Press, p. 697–756.
- Cyr, K.E., and Melosh, H.J., 1993, Tectonic patterns and regional stresses near Venusian coronae: *Icarus*, v. 102, p. 175–184.
- DeLaughter, J.E., and Jurdy, D.M., 1999, Corona classification by evolutionary stage: *Icarus*, v. 139, p. 81.
- DeShon, H.R., Young, D.A., and Hansen, V.L., 2000, Geologic evolution of southern Rusalka Planitia, Venus: *Journal of Geophysical Research*, v. 105, p. 6983–6995.
- Ferrill, D.A., Wyrick, D.Y., Morris, A.P., Sims, D.W., and Franklin, N.M., 2004, Dilational fault slip and pit chain formation on Mars, *GSA Today*, v. 14, p. 4–12.
- Ford, J.P., Plaut, J.J., Weitz, C.M., and 5 others, 1993, Guide to Magellan image interpretation: Pasadena, Calif., National Aeronautics and Space Administration, Jet Propulsion Laboratory, California Institute of Technology, 287 p.
- Ghent, R.R., and Hansen, V.L., 1999, Structural and kinematic analysis of eastern Ovda Regio, Venus—Implications for crustal plateau formation: *Icarus*, v. 139, p. 116–136.
- Ghent, R.R., and Tibuleac, I.M., 2002, Ribbon spacing in Venusian tessera—Implications for layer thickness and thermal state: *Geophysical Research Letters*, v. 29, no. 20, p. 994–997.
- Gilmore, M.S., Collins, G.C., Ivanov, M.A., Marinangeli, L.,

- and Head, J.W., 1998, Style and sequence of extensional structures in tessera terrain, *Venus: Journal of Geophysical Research*, v. 103, no. E7, p. 16,813–16,840.
- Gilmore, M.S., Ivanov, M.I., Head, J., and Basilevsky, A., 1997, Duration of tessera deformation on Venus: *Journal of Geophysical Research*, v. 102, p. 13,357–13,368.
- Grimm, R.E., 1994, Recent deformation rates on Venus: *Journal of Geophysical Research*, v. 99, no. E11, p. 23,163–23,171.
- Guest, J.E., Bulmer, M.H., Aubele, J.C., and 6 others, 1992, Small volcanic edifices and volcanism in the plains on Venus: *Journal of Geophysical Research*, v. 97, p. 15,949–15,966.
- Guest, J.E., and Stofan, E.R., 1999, A new view of the stratigraphic history of Venus: *Icarus*, v. 139, p. 55–66.
- Hamilton, W.B., 2005, Plumeless Venus has ancient impact-accretionary surface, *in* Foulger, G.R., Natland, J.H., Presnall, D.C., and Anderson, D.L., eds., *Plates, plumes, and paradigms: Geological Society of America Special Paper 388*, p. 781–814.
- Hamilton, V.E., and Stofan, E.R., 1996, The geomorphology and evolution of Hecate Chasma, *Venus: Icarus*, v. 121, p. 171–194.
- Hansen, V.L., 2000, Geologic mapping of tectonic planets: *Earth and Planetary Science Letters*, v. 176, p. 527–542.
- Hansen, V.L., 2005, Venus's shield terrain: *Geological Society of America Bulletin*, v. 117, no. 5/6, p. 808–822.
- Hansen, V.L., 2006, Geologic constraints on crustal plateau surface histories, Venus—The lava pond and bolide impact hypotheses: *Journal of Geophysical Research*, v. 111, no. E11010 (doi:10.1029/2006JE002714).
- Hansen, V.L., Banks, B.K., and Ghent, R.R., 1999, Tessera terrain and crustal plateaus, *Venus: Geology*, v. 27, p. 1071–1074.
- Hansen, V.L., and DeShon, H.R., 2002, Geologic map of the Diana Chasma quadrangle (V-37), *Venus: U.S. Geological Survey Geologic Investigations Series I-2752*, scale 1:5,000,000 [<http://geopubs.wr.usgs.gov/i-map/i2752/>].
- Hansen, V.L., Phillips, R.J., Willis, J.J., and Ghent, R.R., 2000, Structures in tessera terrain, Venus—Issues and answers: *Journal of Geophysical Research*, v. 105, p. 4135–4152.
- Hansen, V.L., Tharalson, E.R., McDaniel, K.M., and 2 others, 2008, The coronae conundrum—Results from detailed mapping of Agnesi quadrangle, (V-45; 25-50S/30-60E), *Venus [abs.]: Lunar and Planetary Science*, v. XXXIX, abstract 2325 [PDF].
- Hansen, V.L., and Willis, J.J., 1996, Structural analysis of a sampling of tesserae—Implications for Venus geodynamics: *Icarus*, v. 123, no. 2, p. 296–312.
- Hansen, V.L., and Willis, J.J., 1998, Ribbon terrain formation, southwestern Fortuna Tessera, Venus—Implications for lithosphere evolution: *Icarus*, v. 132, p. 321–343.
- Hansen, V.L., Willis, J.J., and Banerdt, W.B., 1997, Tectonic overview and synthesis, *in* Bouger, S.W., Hunten, D.M., and Phillips, R.J., eds., *Venus II: Tucson, University of Arizona Press*, p. 797–844.
- Hansen, V.L. and Young, D.A., 2007, Venus's evolution—A synthesis, *in* Cloos, M., Carlson, W.D., Gilbert, M.C., Liou, J.G., and Sorensen, S.S., eds., *Convergent Margin Terranes and 6 Associated Regions—A Tribute to W.G. Ernst: Geological Society of America, Special Paper 419*, p. 255–273 (doi: 10.1130/2006.2419 13).
- Hauck, S.A., Phillips, R.J., and Price, M.H., 1998, Venus—Crater distribution and plains resurfacing models: *Journal of Geophysical Research*, v. 103, no. 6, p. 13,635–13,642.
- Head, J.W., and Basilevsky, A.T., 1998, Sequence of tectonic deformation in the history of Venus—Evidence from global stratigraphic relations: *Geology*, v. 26, p. 35–38.
- Herrick, R.R., 1994, Resurfacing history of Venus: *Geology*, v. 22, p. 703–706.
- Herrick, R.R., and Sharpton, V.L., 2000, Implications from stereo-derived topography of Venesian impact craters: *Journal of Geophysical Research*, v. 105, p. 20,245–20,262.
- Herrick, R.R., Sharpton, V.L., Malin, M.C., Lyons, S.N., and Feely, K., 1997, Morphology and morphometry of impact craters, *in* Bouger, S.W., Hunten, D.M., and Phillips, R.J., eds., *Venus II: Tucson, University of Arizona Press*, p. 1015–1046.
- Ivanov, M.A., and Head, J.W., 1996, Tessera terrain on Venus—A survey of the global distribution, characteristics, and relation to surrounding units from Magellan data: *Journal of Geophysical Research*, v. 101, no. 6, p. 14,861–14,908.
- Izenberg, N.R., Arvidson, R.E., and Phillips, R.J., 1994, Impact crater degradation on Venesian plains: *Geophysical Research Letters*, v. 21, p. 289–292.
- Janes, D.M., and Squyres, S.W., 1995, Viscoelastic relaxation of topographic highs on Venus to produce coronae: *Journal of Geophysical Research*, v. 100, p. 21,173–21,187.
- Janes, D.M., Squyres, S.W., Bindschadler, D.L., and 3 others, 1992, Geophysical models for the formation and evolution of coronae on Venus: *Journal of Geophysical Research*, v. 97, p. 16,055–16,068.
- Kirk, R.L., Soderblom, L.A., and Lee, E.L., 1992, Enhanced visualization for interpretation of Magellan radar data—Supplement to the Magellan special issue: *Journal of Geophysical Research*, v. 97, p. 16,371–16,381.
- Koch, D.M., and Manga, M., 1996, Neutrally buoyant diapirs—A model for Venus coronae: *Geophysical Research Letters*, v. 23, p. 225–228.
- Lipman, P.W., 2000, Calderas, *in* Sigurdson, H., Houghton, B., McNutt, S.R., Rymer, H., and Stix, J., eds., *Encyclopedia of Volcanoes: San Diego, Academic Press*, p. 643–661.
- Mackwell, S.J., Zimmerman, M.E., and Kohlstedt, D.L., 1998, High-temperature deformation of dry diabase with application to tectonics on Venus: *Journal of Geophysical Research*, v. 102, p. 975–984.
- McDaniel, K.M., and Hansen, V.L., 2005, Circular lows, a genetically distinct subset of coronae? [abs.]: *Lunar and Planetary Science*, v. XXXVI, abstract 2367 [PDF].
- McGill, G.E., 2004, Tectonic and stratigraphic implications of the relative ages of Venesian plains and wrinkle ridges: *Icarus*, v. 172, p. 603–612.
- McGill, G.E., and Campbell, B.A., 2004, Ages of Venesian ridge belts relative to regional plains [abs.]: *Lunar and Planetary Science*, v. XXXVI, abstract 1143 [PDF].
- McKinnon, W.B., Zahnle, K.J., Ivanov, B.A., and Melosh, H.J., 1997, Cratering on Venus—Models and observations, *in*

- Bouger, S.W., Hunten, D.M., and Phillips, R.J., eds., *Venus II: Tucson, University of Arizona Press*, p. 969–1014.
- Namiki, N., and Solomon, S.C., 1994, Impact crater densities on volcanoes and coronae on Venus—Implications for volcanic resurfacing: *Science*, v. 265, p. 929–933.
- Nunes, D.C., Phillips, R.J., Brown, C.D., and Dombard, A.J., 2004, Relaxation of compensated topography and the evolution of crustal plateaus on Venus: *Journal of Geophysical Research*, v. 109 (doi:10.1029/2003JE002119).
- Okubo, C.H., and S.J. Martel, 1998, Pit crater formation on Kilauea volcano, Hawaii: *Journal of Volcanology and Geothermal Research*, v. 86, p. 1–18.
- Parmentier, E.M., and Hess, P.C., 1992, Chemical differentiation of a convecting planetary interior—Consequences for a one plate planet such as Venus: *Geophysical Research Letters*, v. 19, p. 2015–2018.
- Phillips, R.J., 1993, The age spectrum of the Venusian surface [abs.]: *Eos, Transactions of the American Geophysical Union, Supplement*, v. 74, no. 16, p. 187.
- Phillips, R.J., and Hansen, V.L., 1994, Tectonic and magmatic evolution of Venus: *Annual Reviews of the Earth and Planetary Sciences*, v. 22, p. 597–654.
- Phillips, R.J., and Hansen, V.L., 1998, Geological evolution of Venus—Rises, plains, plumes and plateaus: *Science*, v. 279, p. 1492–1497.
- Phillips, R.J., and Izenberg, N.R., 1995, Ejecta correlations with spatial crater density and Venus resurfacing history: *Geophysical Research Letters*, v. 22, no. 12, p. 1517–1520.
- Phillips, R.J., Raubertas, R.F., Arvidson, R.E., and 4 others, 1992, Impact crater distribution and the resurfacing history of Venus: *Journal of Geophysical Research*, v. 97, p. 15,923–15,948.
- Price, M., and Suppe, J., 1994, Mean age of rifting and volcanism on Venus deduced from impact crater densities: *Nature*, v. 372, p. 756–759.
- Price, M.H., Watson, G., and Brankman, C., 1996, Dating volcanism and rifting on Venus using impact crater densities: *Journal of Geophysical Research*, v. 101, no. 2, p. 4637–4671.
- Pritchard, M.E., Hansen, V.L., and Willis, J.J., 1997, Structural evolution of western Fortuna Tessera, Venus: *Geophysical Research Letters*, v. 24, p. 2339–2342.
- Sandwell, D.T., Johnson, C.L., and Suppe, J., 1997, Driving forces for limited tectonics on Venus: *Icarus*, v. 129, no. 1, p. 232–244.
- Schaber, G.G., Strom, R.G., Moore, H.J., and 7 others, 1992, Geology and distribution of impact craters on Venus—What are they telling us?: *Journal of Geophysical Research*, v. 97, p. 13,257–13,302.
- Schubert, G.S., Solomatov, V.S., Tackely, P.J., and Turcotte, D.L., 1997, Mantle convection and thermal evolution of Venus, *in* Bouger, S.W., Hunten, D.M., and Phillips, R.J., eds., *Venus II: Tucson, University of Arizona Press*, p. 1,245–1,288.
- Schultz, R.A., Okubo, C.H., Goudy, C.L., and Wilkins, S.J., 2004, Igneous dikes on Mars revealed by Mars Orbiter Laser Altimeter topography: *Geology*, v. 32, p. 889–892.
- Shankar, B. and Hansen, V.L., 2008, Preliminary global survey of circular lows, A subset of Venusian coronae [abs.]: *Lunar and Planetary Science*, v. XXXIX, abstract 1813 [PDF].
- Sharpton, V.L., 1994, Evidence from Magellan for unexpected deep complex craters in Venus, *in* Dressler, B.O., Grieve, R.A.F., and Sharpton, V.L., eds., *Large meteorite impacts and planetary evolution: Geological Society of America Special Paper 293*, p. 19–27.
- Skinner, J.A., and Tanaka, K.L., 2003, How should map units be defined? [abs.]: *Lunar and Planetary Science*, v. XXXIV, abstract 2100 [PDF].
- Smrekar, S.E., and Stofan, E.R., 1997, Coupled upwelling and delamination—A new mechanism for corona formation and heat loss on Venus: *Science*, v. 277, p. 1289–1294.
- Solomatov, V.S., and Moresi, L.N., 1996, Stagnant lid convection on Venus: *Journal of Geophysical Research*, v. 101, no. 2, p. 4737–4753.
- Solomon, S.C., 1993, The geophysics of Venus: *Physics Today*, v. 46, no. 7, p. 48–55.
- Solomon, S.C., Bullock, M.A., and Grinspoon D.H., 1999, Climate change as a regulator of tectonics on Venus: *Science*, v. 286, no. 87, p. 5437.
- Squyres, S.W., Janes, D.M., Baer, G., and 4 others, 1992, The morphology and evolution of coronae on Venus: *Journal of Geophysical Research*, v. 97, p. 13,611–13,634.
- Steinbach, V., and Yuen, D.A., 1992, The effects of multiple phase transitions on Venusian mantle convection: *Geophysical Research Letters*, v. 19, no. 22, p. 2243–2246.
- Stofan, E.R., Brian, A.W., and Guest, J.E., 2005, Resurfacing styles and rates on Venus—Assessment of 18 Venusian quadrangles: *Icarus*, v. 173, p. 312–321.
- Stofan, E.R., Hamilton, V.E., Janes, D.M., and Smrekar, S.E., 1997, Coronae on Venus—Morphology and origin, *in* Bouger, S.W., Hunten, D.M., and Phillips, R.J., eds., *Venus II: Tucson, University of Arizona Press*, p. 931–968.
- Stofan, E.R., Senske, D.A., and Parker, T.J., 1993, Tectonic features in Magellan data, *in* Ford, J.P., Plaut, J.J., Wietz, C.M., and 5 others, eds., *Guide to Magellan Image interpretation: Pasadena, Calif., National Aeronautics and Space Administration, Jet Propulsion Laboratory, California Institute of Technology*, p. 93–108.
- Stofan, E.R., Sharpton, V.L., Schubert, G., and 4 others, 1992, Global distribution and characteristics of coronae and related features on Venus—Implications for origin and relation to mantle processes: *Journal of Geophysical Research*, v. 97, p. 13,347–13,378.
- Stofan, E.R., Tapper, S., Guest, J.E., and Smrekar, S.E., 2001, Preliminary analysis of an expanded database of coronae on Venus: *Geophysical Research Letters*, v. 28, p. 4267–4270.
- Strom, R.G., Schaber, G.G., and Dawson, D.D., 1994, The global resurfacing of Venus: *Journal of Geophysical Research*, v. 99, p. 10,899–10,926.
- Tanaka, K.L., Moore, H.J., Schaber, G.G., and 9 others, 1994, *The Venus geologic mappers' handbook: U.S. Geological Survey Open-File Report 94–438*.
- Turcotte, D.L., 1993, An episodic hypothesis for Venusian tectonics: *Journal of Geophysical Research*, v. 98, no. E9,

- p. 17,061–17,068.
- Turcotte, D.L., Morein, G., and Malamud, B.D., 1999, Catastrophic resurfacing and episodic subduction on Venus: *Icarus*, v. 139, no. 1, p. 49.
- Vita-Finzi, C., Howarth, R.J., Tapper, S.W., and Robinson, C.A., 2005, Venusian craters, size distribution, and the origin of coronae, in Foulger, G.R., Natland, J.H., Presnall, D.C., and Anderson, D.L., eds., *Plates, plumes, and paradigms: Geological Society of America Special Paper 388*, p. 815–824.
- Watters, T.R., 1988, Wrinkle ridge assemblages on the terrestrial planets: *Journal of Geophysical Research*, v. 93, p. 10,236–10,254.
- Wichman, R.W., 1999, Internal crater modification on Venus—Recognizing crater-centered volcanism by changes in floor morphometry and floor brightness: *Journal of Geophysical Research*, v. 104, p. 21,957–21,977.
- Wilhelms, D.E., 1990, Geologic mapping, in Greeley, R., and Batson, R.M., eds., *Planetary Mapping: New York, Cambridge University Press*, p. 208–260.
- Withjack, M.O., Olsen, P.E., and Schlische, R.W., 1995, Tectonic evolution of the Fundy basin, Canada—Evidence of extension and shortening during passive-margin development: *Tectonics*, v. 14, p. 390–405.
- Withjack, M.O., and Scheiner, C., 1982, Fault patterns associated with domes—An experimental and analytical study: *American Association of Petroleum Geologists Bulletin*, v. 66, no. 3, p. 302–316.
- Withjack, M.O., Schlische, R.W., and Olsen, P.E., 1998, Diachronous rifting, drifting, and inversion on the passive margin of eastern North America—An analogue for other passive margins: *American Association of Petroleum Geologists Bulletin*, v. 82, no. 5A, p. 817–835.
- Zimelman, J.R., 2001, Image resolution and evaluation of genetic hypotheses for planetary landscapes: *Geomorphology*, v. 37, p. 179–199.

Table 1. *Numbers and densities of definite shields (DS) and combined shields (CS), which consist of definite and potential shields, in the Niobe Planitia quadrangle (V-23).*

Centered at lat/long	DS	CS	DS/10 ⁶ km ²	CS/10 ⁶ km ²
23° N./103° E.	402	626	10,500	15,650
21° N./113° E.	167	1,080	4,175	27,000
13° N./111° E.	142	1,347	3,550	33,675
23° N./117° E.	251	1,005	6,275	25,125
13° N./119° E.	271	631	7,078	15,775

Table 2. *V-23 impact craters.*

Name	Latitude (deg N.)	Longitude (deg E.)	Diameter (km)	C density*	Unit Location	Ejecta blanket	Impact halo	Central peak	Rim	Interior flooding	Elevation (km)
Millay	24.4	111.2	48.0	2.86479	st	Y	N	N	Y	Y	6051.33
LiQuingzhao	23.7	94.6	22.8	2.54648	st	Y	Y	Y	Y	Y?	6051.67
Caldwell	23.6	112.4	51.0	3.1831	st	Y	Y	N	Y	N	6051.52
Horner	23.4	97.8	25.2	2.86479	st	Y	N	Y	Y	Y	6051.36
crater a	22.6	94.1	3.0	2.22817	st	Y	N	N	Y	N	6051.43
Kiris	20.9	98.8	13.3	2.22817	st	Y	N	N	Y	Y	6051.67
Zulfiya	18.4	101.9	12.9	2.54648	st	Y	N	N	Y	N	6051.63
Hannah	17.9	102.6	19.8	2.54648	st	Y	N	Y	Y	Y	6051.54
Barrera	16.7	109.4	26.8	3.1831	st	Y	N	Y	Y	Y	6051.67
Ferrier	15.7	111.3	19.1	3.1831	st	Y	N	Y	Y	Y	6051.51
crater b	15.1	116.8	4.5	3.50141	st	Y	N	N	Y	?	6051.63
crater c	13.3	112.8	4.2	1.90986	st	Y	N	N	Y	N	6051.24
Adzoba	12.8	117.0	10.0	3.1831	st	Y	N	N	Y	Y	6051.50
Merit Ptah	11.4	115.6	16.5	2.86479	st	Y	N	N	Y	N	6051.19
Gregory	7.1	95.8	18.0	3.1831	st	Y	N	N	Y	Y	6053.17
Icheko	6.6	97.9	5.9	2.86479	st	Y	N	Y	Y	N	6053.53
Chapelle	6.4	298.3	20.8	2.22817	st	Y	N	Y	Y	Y	6051.86
Abra	6.2	282.91	7.2	2.86479	st	?	?	?	?	?	6055.54
Susanna	6.0	287.75	13.3	3.50141	st, rttO	Y	N	N	Y	N?	6053.37
Hepworth	5.1	289.95	62.6	3.50141	rttO, itbO	Y	N	Y	Y	Y	6054.16
Tsiala	2.9	280.3	16.5	3.81972	rttO	partial	N	Y	Y	Y	6054.83
Doris	2.3	277.0	14.5	3.50141	rttO	minor	N	N	Y	Y	6055.01
deBeauvoir	2.0	283.8	52.5	3.81972	rttO	Y	N	Y	Y	Y	6054.79
Estella	1.1	285.27	18.8	3.50141	rttO	Y	N	Y	Y	Y	6055.06

*Crater density (values from Herrick and others, 1997) at a crater's location (Rho). Value is the density of craters in the neighborhood of the specified crater. This is calculated by counting the number of craters (including the specified crater) within a 1000 km radius circle, and normalizing to give the number of craters per 1×10^6 km².

